Deep–Sea Research II 218 (2024) 105429

Contents lists available at ScienceDirect

Deep-Sea Research Part II

journal homepage: www.elsevier.com/locate/dsr2

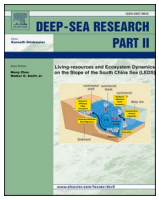

# Ocean-atmosphere-ice processes in the Ross Sea: A review

Pierpaolo Falco [a,b], Giuseppe Aulicino [c], Pasquale Castagno [b,d], Vincenzo Capozzi [c], Paola de Ruggiero [c], Angela Garzia [a,e], Antonino Ian Ferola [c], Yuri Cotroneo [b,c], Alessio Colella [c], Giannetta Fusco [b,c], Stefano Pierini [b,c], Giorgio Budillon [b,c], Enrico Zambianchi [b,c,*], Giancarlo Spezie [c]

[a] Dipartimento di Scienze della Vita e dell'Ambiente, Università Politecnica delle Marche, 60131, Ancona, Italy
[b] CoNISMa (Consorzio Nazionale Universitario per le Scienze del Mare), 00196, Roma, Italy
[c] Dipartimento di Scienze e Tecnologie, Università degli Studi di Napoli "Parthenope", 80143, Napoli, Italy
[d] Dipartimento di Scienze Matematiche e Informatiche, Scienze Fisiche e Scienze della Terra, Università degli Studi di Messina, 98166, Messina, Italy
[e] Dipartimento di Ingegneria Civile, Edile e Ambientale, Università degli Studi di Roma "Sapienza", 00184, Roma, Italy

ARTICLE INFO

Handling Editor: Dr W Smith

*Keywords:*
Ross sea
Antarctic waters
Water masses
Ocean variability
Polynyas
Sea ice

ABSTRACT

The Ross Sea has been the site of extensive investigations since the earliest days of polar exploration. The International Geophysical Year of 1957-58 enhanced research activities with the establishment of scientific stations and the collection of oceanographic observations in the area. While many features of its oceanography, ecology, physics, glaciology, geology, and biogeochemistry are known, recent advances provide new insights into its structure and function, as well as into its relationship to global climate. We present a comprehensive review of the advances of understanding the main processes occurring in the area, such as the formation of dense shelf water and the production of Antarctic Bottom Water (AABW), as well as the main drivers (at both large and local scales) of local dynamics and water mass variability. We also summarize the main modeling applications, which are still limited and need to be improved using high-resolution models and, locally, limited-area models to explain processes driven mainly by thermodynamics and water-mass transformations. The Ross Sea forms the most saline AABW due to the activity of two polynyas in the western sector. A salinity gradient occurs on the shelf, with fresh Low Salinity Shelf Waters concentrated in the eastern Ross Sea, which is influenced by the inflow of fresh water from the Amundsen and Bellingshausen Seas. This freshwater inflow was thought to be the cause of a multi-decadal freshening of the High Salinity Shelf Water, precursor to the AABW, although a rebound in salinity in the Ross Sea has been observed since 2014. The increase in salinity has also affected the production of AABW, with the respective rebound occurring almost simultaneously.

## 1. Introduction

The Ross Sea is a vast, deep bay in the southwestern Pacific Ocean bounded by Marie Byrd Land to the east, Victoria Land to the west and the Ross Ice Shelf (RIS) to the south (Fig. 1). Intricate interactions between atmosphere, ocean, sea ice and ice shelf make the Ross Sea a dynamic and complex region with significant implications for regional and global climate. It is the source region of the Antarctic Bottom Water (AABW), the most abundant and densest water mass in the deep ocean (Johnson, 2008). Together with the Weddell Sea, these regions contribute ca. 80–90% of the global AABW (Orsi et al., 2002), with approximately 30–40% estimated to originate in the Ross Sea (Johnson, 2008). The AABW feeds the lower cell of the Global Overturning Circulation (Orsi et al., 1999; Lumpkin and Speer, 2007; Marshall and Speer, 2012), supplying oxygen and storing heat and carbon in the abyssal ocean (Johnson, 2008) and playing a key role in the climate system. The Ross Sea AABW originates at the shelf break and slope from the mixing of the cold Dense Shelf Water (DSW), formed on the continental shelf during winter (Budillon et al., 2011; Rivaro et al., 2015).

The modern era of observations in the Ross Sea dates back to the late 1950s and early 1960s when first indications of shelf water salinity values in the western sector were reported (Newson et al., 1965). Furthermore, insights about the main characteristics (temperature maximum at intermediate depths and oxygen minimum) of the modified

* Corresponding author. Dipartimento di Scienze e Tecnologie, Università degli Studi di Napoli "Parthenope", 80143 Napoli, Italy
*E-mail address:* enrico.zambianchi@uniparthenope.it (E. Zambianchi).

https://doi.org/10.1016/j.dsr2.2024.105429
Received 26 April 2024; Received in revised form 24 September 2024; Accepted 11 October 2024
Available online 11 October 2024

Circumpolar Deep Water (mCDW) were reported. Jacobs et al. (1970) identified and labeled the Ice Shelf Water (ISW) for the first time in the Ross Sea and measured temperatures as low as −2.13 °C close to the RIS front and a difference in salinity between the eastern and western RIS edge. They also described two different types of AABW: a more saline one due to the contribution of High Salinity Shelf Water (HSSW) observed in the western Ross Sea and a fresher one, due to the entrainment of ISW and CDW along the slope in the eastern Ross Sea. Important advances in the knowledge of DSW formation processes and the dynamics of these water masses were made between 1976 and 1985 when both hydrological and current measurements provided a description of the sub-surface circulation in the central area of the Ross Sea and in the vicinity of the RIS (Pillsbury and Jacobs, 1985). Chemical tracers were used to study the role played by the DSW in ventilating the abyss of the Southern Ocean (Jacobs and Fairbanks,1985) and the use of chlorofluorocarbon contributed to estimate the renewal time of the Ross Sea water masses (Trumbore et al., 1991; Rivaro et al., 2004).

During the following two decades, research activities in the Ross Sea included a number of multidisciplinary projects aimed to fill the main gaps in understanding the physical, bio-geo-chemical and coupled processes. The "Climatic Long-term Interactions for Mass Balance in Antarctica" (CLIMA) project provided insights into the physical processes (e.g., on DSW formation, spreading dynamics, and exchange with the Southern Ocean). Furthermore, such information was integrated with biogeochemical observations, mainly concentrated on the western sector of the Ross Sea and RIS area. Long-term observations and model simulations provided an understanding of the variability (both spatial and temporal) of the main Ross Sea water masses, of the vertical circulation and its relationship with the marine ecosystem (Spezie and Manzella, 1998), A permanent marine observatory was established in 2009 (Castagno et al., 2017, 2019), generating the longest time series ever collected in this area. Recent projects have extended into the eastern sector of the Ross Sea, a crucial area for the mass balance and especially the salt balance of the basin (Silvano et al., 2020; Jacobs et al., 2022). The deployment of Argo floats equipped with an ice-sensing system began in 2020 and the data are revealing new aspects and describing the winter thermohaline evolution of the water column in important areas of the Ross Sea, such as the Terra Nova Polynya (TNB) and the RIS polynya. In 2010 oceanographic studies began through a series of borehole expeditions (Stevens et al., 2020) to collect data within the RIS cavity, from the rim to the grounding line.

The availability of time series has revealed the presence of substantial variability that is related to atmospheric teleconnections. For example, during the past 60 years, the Ross Sea DSW has undergone a near-linear salinity decrease (Jacobs et al., 2022), although a rebound in salinity was observed from 2016 to 2019 (Castagno et al., 2019; Silvano et al., 2020). The freshening is thought to be caused by a growing imbalance in the amount of meltwater from thinning ice shelves and increased iceberg calving in the upstream Amundsen and Bellingshausen Seas (Jacobs et al., 2022). The rebound has been attributed to a combination of positive Southern Annular Mode (SAM) and negative Southern Oscillation Index (SOI) that weakened the Amundsen Sea Low (ASL) and the Easterlies, thus reducing the volume of sea ice imported into the eastern Ross Sea that triggered an increase in the local sea ice formation (Silvano et al., 2020). The Ross Sea AABW freshening affects the AABW characteristics. In recent decades the most dramatic salinity and density changes in the AABW have been observed in the Pacific and Australian Antarctic Basins, which are primarily sourced from the Ross Sea (van Wijk and Rintoul, 2014; Silvano et al., 2020; Gunn et al., 2023). Changes in the Ross Sea DSW affect the Ross Sea AABW properties

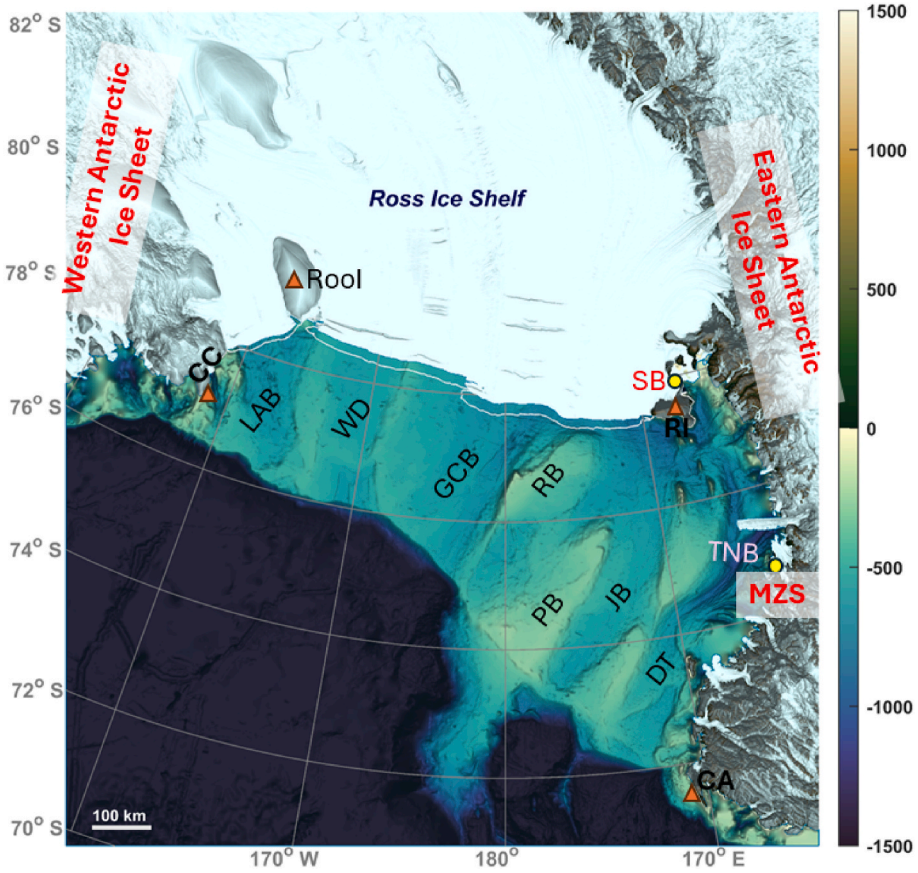


**Fig. 1.** Regional bathymetry of the Ross Sea continental shelf. The main topographic structures are reported: DT, Drygalski Trough, JB Joides Basin, PB Pennel Bank, RB Ross Bank, GCB Glomar Challenger Basin, WD Whales Deep, LAB Little American Basin. The orange triangles on the map indicate: CA Cape Adare, RI Ross Island, RooI Roosevelt Island, CC Cape Colbeck. The yellow dots indicate the position of: MZS Mario Zucchelli Station and SB Scott Base.

(Silvano et al., 2020) and formation rate (Gunn et al., 2023), and these propagate throughout the global ocean and affect stratification (Heuzé et al., 2013), the rate of oxygen supply (Schmidtko et al., 2017), sea level, heat content, and the atmospheric carbon dioxide concentrations on centennial to millennial timescales (Ferrari et al., 2014). Changes in the Ross Sea DSW might also weaken the lower limb of the abyssal overturning circulation and reduce deep ocean oxygen content (Gunn et al., 2023).

This paper aims to provide a view of the dynamics, variability and water mass formation in the Ross Sea, including the large scale and main modes of climatic variability affecting the Ross Sea, an overview of the atmospheric circulation, large-scale and local variability of sea ice concentrations, the RIS, and conclude with a summary of key gaps in our understanding of the Ross Sea.

## 2. Atmospheric circulation

In the past 15-years, several studies have described the atmospheric circulation of the Ross Sea region. Cohen et al. (2013) characterized the synoptic climatology of this area, providing the first climatological categorization of the atmospheric circulation patterns (1979–2011). Six different synoptic types were extracted from a cluster analysis involving daily 1000-hPa geopotential height data. All of the patterns, except one that depicts a purely zonal configuration, are characterized by the presence of low-pressure systems located near 60°S in different sectors of Ross, Amundsen and Bellingshausen Seas (Cohen et al., 2013). The seasonal variation of the identified synoptic types reflects the zonal displacement of the Amundsen Sea Low (Fogt et al., 2012). The synoptic type resembling the Amundsen Sea Low (ASL) configuration is more frequent in austral summer and autumn, while the synoptic type characterized by a low-pressure system in the Ross Sea (L-R) is more prevalent in spring and winter. This suggests that the region of cyclonic circulation moves eastward toward the Bellingshausen Sea during summer and autumn and westward toward the Ross Sea in winter and spring. In addition, Cohen et al. (2013) showed that the L-R synoptic configuration is negatively correlated with the Southern Annular Mode (SAM) and the Southern Oscillation Index (SOI), whereas the occurrence of the meteorological scenario associated with a low-pressure center over the Amundsen-Bellingshausen Seas is positively correlated with the SOI and the SAM. Moreover, Cohen et al. (2013) found a strong relationship between some of the identified circulation patterns and the local climate variability. A significant fraction (~30%) of the precipitation observed at Roosevelt Island ice core site (80°S, 160°W, 550 m above sea level) is related to the occurrence of L-R circulation type. On short-term time scales, Sinclair et al. (2010) analyzed the variability in snowfall accumulation from November 2007 to October 2008 at two sites located along the western margin of the RIS and investigated the main atmospheric patterns that drive precipitation events. The results showed that the moisture supply comes from a wide spectrum of cyclonic areas (some of them traveling around the continent in circumpolar westerlies and other stationing over the Ross Sea) and also by mesocyclones that form locally over the RIS or the Ross Sea delivering short snowfall events. Fonseca et al. (2023) investigated the atmospheric factors that control the spatial extension of the Terra Nova Bay Polynya (TNBP). Using ERA-5 reanalysis, satellite-derived and in situ meteorological data, they found that katabatic wind episodes and warm and moist air intrusions from low-latitudes are the main factors that drive the variability of the TNBP's size. The synoptic configuration underlying the occurrence of the katabatic events is associated with a westward shift of the ASL and a ridge over Antarctica, which results in a rise of pressure gradient and a strengthening of the off-shore winds. The large-scale pattern that stimulates warm and moist air advection is characterized by a deepening of the ASL and by a ridge over Antarctica, a pattern that resembles the negative phase of the SAM (Fonseca et al., 2023).

In recent decades substantial efforts have been devoted to the study of the atmospheric and climate variability of the Pacific sector of the Southern Ocean (PSSO) and Antarctica. The whole area, and in particular the Ross Sea, is a relevant location of atmospheric-ocean-ice interactions, where relatively small-scale processes have a disproportionate impact on global ocean circulation (Malyarenko et al., 2023). Three major atmospheric circulation patterns modulate the environmental variability of the region: the SAM, the El-Niño Southern Oscillation (ENSO) and the Inter-Decadal Pacific Oscillation (IPO). The SAM is a zonally symmetric or annular pattern of atmospheric pressure (Fig. 2a) and captures a large portion of the low-frequency variability of the Southern Hemisphere extra-tropics, providing a robust measure of the strength and position of the westerly winds through the difference of zonal mean sea level pressure between 40°S and 60°S (Thompson and Wallace, 2000; Cerrone et al., 2017; Cerrone and Fusco, 2018). Positive phases of the SAM are generally associated with above-average temperatures over the Antarctic Peninsula and colder conditions over East Antarctica, due to an increase of pressure gradient between mid- and polar latitudes, and a declining transport of heat and moisture and a reduction in katabatic flow (Thompson and Solomon, 2002a; Marshall and Thompson, 2016). Since the 1950s, a positive trend of the SAM (which means decreasing pressure over Antarctica) has been observed, especially in summer and marginally during autumn. This behaviour of the SAM has been partly attributed to an increase in the amount of greenhouse gasses in the atmosphere and to stratospheric ozone depletion (Arblaster et al., 2011). The positive SAM trend resulted in a general increase of equatorward heat flux along the Antarctic margin, except for the western Ross Sea region, which experienced an unusual poleward heat flux that drove moisture and heat across the RIS (Marshall and Thompson, 2016).

The atmospheric variability of the Ross Sea region is also explained by the Rossby wave propagation associated with ENSO. More specifically, Rossby wave trains excited by anomalies in the tropical deep convection during ENSO events are synthesized by the Pacific South American (PSA) pattern (Fig. 2b). The latter represents a wave train extending from the Central Pacific Ocean to the Amundsen and Weddell Seas (Irving and Simmonds, 2016). The PSA is commonly analyzed in terms of two Empirical Orthogonal Function (EOF) modes, known as PSA-1 and PSA-2. The negative (positive) phase of PSA-1 and PSA-2 depicts atmospheric scenarios similar to El-Niño (La-Niña) conditions (Mo, 2000). According to Marshall and Thompson (2016), the positive phase of PSA-1 determines anomalous anticyclonic wind anomalies in the South Pacific around ~120°W. During the positive polarity of the PSA-2, the anticyclonic area moves to ~150°W in the Ross Sea, generating a dipole over the RIS. In this configuration, the western RIS experiences an increase in the transport of moist air masses, whereas the eastern RIS is affected by an enhanced katabatic flow. The coupling between specific ENSO and SAM phases has an impact on sea ice in the western Ross Sea (Stammerjohn et al., 2008). In particular, the combination of negative SAM and El-Niño events leads to an increase of poleward heat flux and, therefore, to a reduction of sea ice, whereas when a positive SAM in conjunction with positive ENSO (i.e. La-Niña conditions) occurs, an increase in sea ice in the western Ross Sea is observed due to a decline in poleward heat flux.

SAM and PSA-1 patterns both affect the state of the Amundsen Sea Low (ASL), a semi-permanent cyclonic system in the Ross-Amundsen Sea. The ASL is the most relevant of the three low-pressure areas around Antarctica, associated with wave number 3 circulation (Turner et al., 2013; Raphael and Hobbs, 2014). The strength and the position of the ASL are strongly linked to the SAM (especially during the austral autumn) and to the ENSO (particularly during austral winter and spring). Specifically, positive SAM and/or La Niña episodes determine a strengthening of the ASL, whereas the opposite polarities (i.e. negative SAM and El-Niño events) lead to a weakening (Turner et al., 2013). The climatological position of the ASL has a seasonal dependence: the ASL center moves from ~110°W during austral summer to ~150°W in winter (Turner et al., 2013). The ASL has a remarkable impact on the

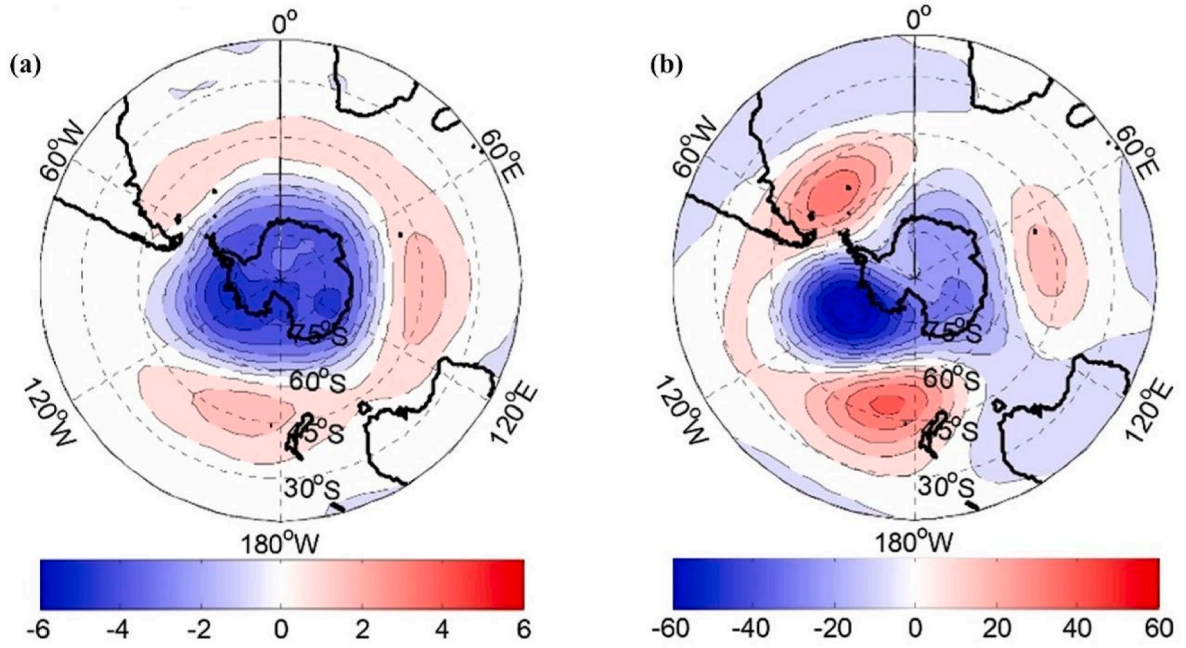


**Fig. 2.** Spatial pattern generated by regressing the unfiltered and unnormalized sea level pressure anomalies (in hPa) into the SAM (panel a) and the 500-hPa geopotential height anomalies (in geopotential meters) into the PSA (panel b). Figure adapted from Cerrone and Fusco (2018).

environmental conditions over the Ross, Amundsen and Bellingshausen seas, as well as across the Antarctic Peninsula and Western Antarctic (e.g. Ding and Steig, 2013; Steig et al., 2015). The main signature of the ASL in the meteorological regime of the RIS lies in the wind field, which is dominated by southerly winds that force flow off the shelf, enhancing sea ice production. There has also been a great deal of research on the relationship between ENSO and variability in depth and location of the ASL. The first evidence of linkages was provided by Cullather et al. (1996), who found that between 1980 and 1990 the ASL moved 1400 km east during El-Niño events compared to the average climatological location. La-Niña conditions generally result in a deepening and in a westward movement of the low, whereas during El-Niño it's the opposite (i.e. weakening and eastward movement; Bertler et al., 2004). The process by which the ENSO leads to the ASL anomaly does not occur synchronously: typically, the ENSO reaches the greatest strength in summer and decays in autumn, whereas the ASL anomaly in response to ENSO is more evident during autumn than summer (Jin and Kirtman, 2009; Yiu and Maycock, 2019). The mechanisms that are behind the delayed responses of the atmospheric circulation anomaly over the Amundsen Sea to the ENSO have been clarified by Lee and Jin (2023). In particular, ENSO-induced perturbations (represented by a barotropic Rossby wave propagation) found an ideal basic state for a southward displacement towards the Amundsen Sea only in May when a path develops near the exit region of the subtropical jet.

On a decadal scale, the atmospheric variability of the PSSO is strongly conditioned by the IPO, a long-term oscillation of the sea surface temperature (SST) that is closely related to the Pacific Decadal Oscillation (PDO). The latter can be defined as the leading EOF of the SST variability in the north Pacific, whereas the IPO synthesizes a spatial pattern of SST reminiscent of ENSO but wider in meridional scale (Henley et al., 2015). The positive phase of IPO is characterized by warmer SSTs (up to 0.5 °C) in the central and eastern equatorial Pacific, whereas in the north and south Pacific, the SSTs are cooler (up to 0.5°C; Henley et al., 2015; Purich et al., 2016). Such a scenario is associated with an increase in the frequency of occurrence of El-Niño events. Cooler equatorial Pacific SSTs and strengthened trade winds are typical features of the negative IPO phase. The SST spatial patterns generally last for 20–30 years and can exert an influence on the amplitude and frequency of the Pacific-Antarctic teleconnections (Li et al., 2021). A negative IPO results in colder SSTs in the Ross Sea, as well as in the Amundsen and Bellingshausen Seas, while the positive polarity of this teleconnection leads to warmer SSTs (Henley et al., 2015). From the late 1990s to the mid-2010s, the negative phase of IPO prevailed and, therefore negative SST anomalies were observed in the Central Pacific. This SST pattern and the corresponding variations in convection and upper-level vorticity in the tropical Pacific area excited a Rossby wave train, with a negative low-pressure anomaly over the Amundsen and Bellingshausen seas (Clem and Fogt, 2015; Purich et al., 2016). This Rossby wave train emerged in all seasons, except in austral summer and might be linked to the negative polarity of PSA patterns driven by La-Niña events, whose frequency of occurrence raised along with an IPO negative phase (Purich et al., 2016; Clem and Fogt, 2015). The persistence of the negative IPO-phase between the late 1990s and mid-2010s and the resulting Rossby wave train determined an intensification of ASL up to 4 hPa (Meehl et al., 2016). The IPO-driven pressure anomaly patterns are characterized by a stronger north-south gradient and greater zonal asymmetry over the South Pacific compared to ENSO-related events (Clem and Fogt, 2015; Meehl et al., 2016). Such differences have been attributed to the positive SST anomalies in the South Pacific Convergence Zone (SPCZ), which initiated a Rossby wave dynamics independent from those occurring in the equatorial Pacific (Joughin et al., 2014; Clem and Fogt, 2015; Clem et al., 2016). The wave trains initiated by the SPCZ cause the formation of an anomalous cyclonic system over the Ross Sea.

An additional contribution to the atmospheric variability of the investigated area comes from Atlantic and Indian Ocean teleconnections. On the interannual scale, anomalous tropical Atlantic warming can indirectly trigger a Rossby wave pathway from the subtropical Atlantic to the Amundsen-Bellingshausen Seas and drive a deepening of the ASL and a transition of the SAM to its positive phase (Li et al., 2014, 2015; Simpkins et al., 2014). Some teleconnection patterns impacting the atmospheric dynamics of the Ross Sea region and surrounding areas are linked to anomalies of the convective heating in the Indian Ocean. Several studies (Saji et al., 2005; Cai et al., 2011; Nuncio and Yuan, 2015; Wang et al., 2019) have demonstrated that the Indian Ocean Dipole can lead a Rossby wave train towards southern latitudes

that influence the Antarctic atmospheric variability through its zonal wavenumber 3 pattern during austral spring.

## 3. Sea ice

### 3.1. Sea ice extent

The sea ice annual cycle represents one of the largest seasonal changes on the planet (Wadhams et al., 2018) which significantly impacts the climate system and ecosystems at both global and regional scales (Ayres et al., 2022; Swadling et al., 2023). The presence and variability of sea ice cover determine several basic characteristics of the polar regions. It affects the exchange of heat, energy, mass and momentum between the ocean and the atmosphere (Aulicino et al., 2019), the freshwater fluxes that impact overturning circulation (Meccia et al., 2023; Ferola et al., 2023) and the light penetration that drives biological processes and polar food webs (Castellani et al., 2018; Massom and Stammerjohn, 2010). Sea ice formation and melting alter the buoyancy structure of the ocean, modulate the production of dense waters and regulate the aerosol and gas import/export between the ocean and the atmosphere (McFarquhar et al., 2021; Heil et al., 2023). Therefore, monitoring the variability in Sea Ice Concentration (SIC) and Extent (SIE) over the Antarctic ocean sectors is crucial for understanding and forecasting Earth's climate (Parkinson and Cavalieri, 2012).

A dramatic reversal in the Antarctic sea ice has been observed since 2016 from gradual increases to rapid decreases (Parkinson, 2019; Hobbs et al., 2024). The multidecadal positive trend that culminated in record high SIE in 2014 has been followed by a series of exceptional minimums, with four record-breaking low sea ice summers in the last eight years and a doubled standard deviation of summer records in the last fifteen years (Raphael and Handcock, 2022; Liu et al., 2023; Hobbs et al., 2024). A new minimum in Antarctic SIE (1.77,$10^6$ $km^2$) was observed on February 19, 2023, accounting for 36% less sea ice than the 1979–2022 average minimum (Purich and Doddridge, 2023). In addition, a lower sea ice cover has been observed also during the autumn and winter advance, such as in 2023 which led to a maximum SIE that was $1 \times 10^6$ $km^2$ lower than the previous year (Hobbs et al., 2024). Despite the limited length of the SIE time series and the paucity of ocean observations under sea ice, several authors point out that these abrupt changes cannot be ascribed only to anomalous atmospheric fluctuations and the confluence of regional atmospheric modes, suggesting that the decadal Southern Ocean subsurface warming was an additional and important driver of the lower sea ice (Dotto et al., 2018; Eayrs et al., 2021; Purich and Doddridge, 2023; Hobbs et al., 2024). Regardless of the causes, a shift into a new low-extent regime of sea ice may be in progress in which the underlying processes controlling SIE may have undergone alterations. This could manifest in a sea ice cover more closely linked to subsurface ocean conditions, a change in seasonal interactions between sea ice and the ocean mixed layer, and a distinct response to climate drivers such as SAM phases (Eayrs et al., 2021; Purich and Doddridge, 2023; Hobbs et al., 2024).

A similar change in SIE tendency was observed in the Ross Sea where the increase recorded during the satellite era was replaced by a series of minimum values since 2014 (Fig. 2) and by an abrupt reduction of maximum extent in 2023 (Parkinson, 2019; Swathi et al., 2023).

The Ross Sea accounts for most ($13.7 \pm 3.6 \times 10^3$ $km^2$ per year) of the overall SIE increase around Antarctica ($17.5 \pm 4.1 \times 10^3$ $km^2$ per year) observed between 1979 and 2014 (Hobbs et al., 2016). The SIE trend in the Ross Sea is also the only statistically significant one of all Antarctic sub-regions. This trend cannot be explained by natural variability alone and must involve external anthropogenic forcing mechanisms (Yuan et al., 2017). On the other hand, in the Ross Sea climate simulations and satellite retrievals have frequently exhibited significant discrepancies, and the underlying mechanisms driving sea ice variability remain poorly understood (Lecomte et al., 2017). The region is spatially complex, being characterized by the coexistence of important polynyas (i.e., Ross, McMurdo, Terra Nova Bay), major ice shelves (Ross, Nansen) and a glacier tongue (Drygalski), whose integrity determines the fate of sea ice in the region (Heil et al., 2023).

At shorter time scales, the atmosphere emerges as the primary driver influencing sea ice distribution across the Ross Sea (Hobbs et al., 2024). Wind affects freezing and melting rates and drives sea ice motion, especially in the outer pack where SIC is lower and sea ice is less compact. In the inner areas, sea ice distribution is also shaped by local circulation and eddies. However, SIE is generally reduced by northerly winds which push sea ice towards the Antarctic continent, generating thicker ice and ridges (Massom et al., 2008). Conversely, southerly winds push the ice edge further north increasing SIE and favoring freezing (in winter) and surface warming (in summer) over polynyas and open leads (Hobbs et al., 2024). Farooq et al. (2020) found that the directional constancy of sea ice drift is closely related to the wind fields in the western Ross Sea and that large-scale sea ice motion is predominantly wind-driven while ocean currents play a minor role.

Lecomte et al. (2017) demonstrated that in the Ross Sea the heat trapped below the ocean mixed layer is comparable to the latent heat storage due to the long-term changes in sea ice volume, suggesting that the observed sea ice increase could have been forced by a reorganization of energy within the near-surface ice-ocean system. They also argued that the initial perturbation necessary to trigger this mechanism could be provided by a combination of external forcing on sea ice dynamics (through changes in wind regimes) and ocean freshwater balance (i.e., through increased precipitation and/or ice sheet melting).

Ocean and atmosphere processes drive the seasonal cycle of sea ice in the Ross Sea (Fig. 3) which is characterized by a consistent minimum in February, with a 42-year average of $0.619 \times 10^6$ $km^2$ between 1979 and 2020 (Swathi et al., 2023) and a winter maximum that varies between July and November (Parkinson, 2019), with an average of $3.39 \times 10^6$ $km^2$ between 1979 and 2020 (Swathi et al., 2023). Despite the increase in SIE prior to 2016, the Ross Sea sector experienced an extensive sea ice loss with record low in summer 2017 and 2022 (DuVivier et al., 2024), and in winter 2017 and 2023 (Fig. 3). Nonetheless, higher (lower) winter maxima are not necessarily followed by higher (lower) summer extents, suggesting that the atmospheric and oceanic conditions play a major role in driving seasonal increases/decays (Heil et al., 2023). ENSO and IPO have statistically significant negative correlations with the Ross Sea SIE, whereas SAM shows a statistically significant positive correlation (Swathi et al., 2023). This implies that the SIE decreases (increases) during the warm (cold) phase of ENSO. Sea ice loss in the Ross Sea is possibly caused by a combination of multiple anomalous atmospheric patterns and altered ocean conditions. Recent studies, for example, show that low SIE in the Ross Sea can be sometimes attributed to ocean subsurface warming (Zhang et al., 2022), while in other years to anomalous south-westerly winds that move sea ice offshore, decreasing its regional presence but increasing it to the Pacific sector of the Southern Ocean (Zhang and Li, 2023).

The impact of continental ice melting on sea ice presence in the Ross Sea remains uncertain. By inducing surface freshening and increasing near-surface stratification, meltwater should lead to surface cooling, favoring SIE. However, there is no clear evidence of the magnitude of the sea ice response to meltwater and its impact on sea ice variability (Purich and Doddridge, 2023). Additionally, more icebergs are now present in the Ross Sea, with more important calving events reported in recent years (e.g., Tournadre et al., 2016; Qi et al., 2021; Zahriban Hesari et al., 2023), both affecting the growth, structure and, hence, the persistency of sea ice (Aulicino and Wadhams, 2022).

### 3.2. Sea Ice Thickness

Despite its significance for sea ice mass balance, radiative budget and marine life, little is known about Sea Ice Thickness (SIT) in the Ross Sea. This information is essential for monitoring and better understanding the fate of seasonal sea ice cover, especially in the marginal ice zone

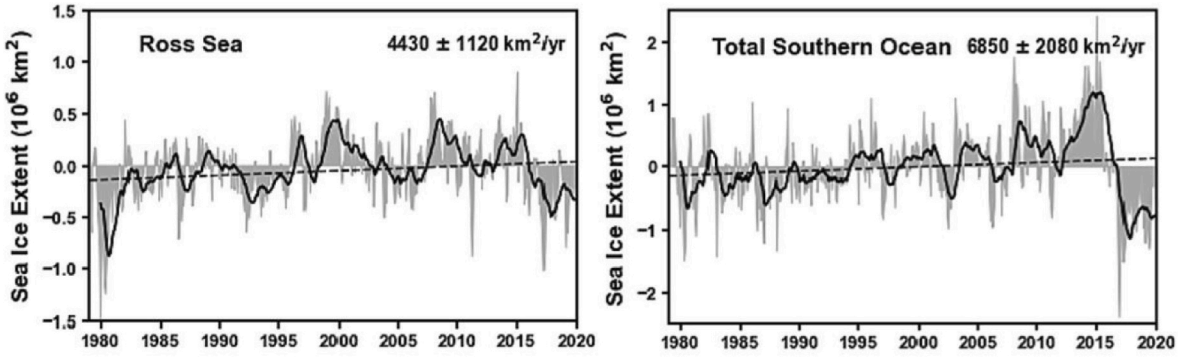


**Fig. 3.** Monthly anomalies and trends of the Sea Ice extent in the Ross Sea (left) and in the whole Southern Ocean (right). Thick black lines show the 12-month running average, and the black dashed line shows the trend (adapted from Swathi et al., 2023).

where it represents an important factor in wave-ice interactions that can impact SIE and its evolution (Wadhams et al., 2018; Vichi, 2022; Womack et al., 2024). To date, SIT estimates rely on satellite retrievals from passive and active microwaves (Kaleschke et al., 2012; Aulicino et al., 2014, 2019; Nihashi et al., 2024) and on the freeboard evaluation from altimeters (Kurtz and Markus, 2012; Paul et al., 2018) or aircraft (Tian et al., 2020). Satellite observations still suffer from significant uncertainties caused by snow cover and small-scale variability of sea ice (Kern and Ozsoy-Çiçek, 2016), and in situ information is extremely sparse and sporadic (Rack et al., 2021) despite their crucial role in validating satellite products and assessing simulated sea ice volume estimations.

However, insights into the SIT distribution in the western Ross Sea were recently provided by airborne measurements (Rack et al., 2021). Data collected during November 2017 revealed a heavily deformed ice regime with a mean thickness of 2.0 ± 1.6 m, much thicker than in the central Ross Sea and more than expected from thermodynamic growth. Maximum thickness was retrieved north of Terra Nova Bay, with values up to 16 m and a mean thickness of the thickest 10% of ice of about 7.6 m (Rack et al., 2021). Similar characteristics were found north of McMurdo Sound, suggesting that ice preferentially grows in deformational ridges over the western Ross Sea concentrating about 43% of the sea ice volume in the area where ridges are more than 3 m. High sea ice deformation also influences the thickness of fast ice (Langhorne et al., 2023). An inventory of fast ice thickness gave a mean of 2.6 ± 1.0 m and an overall mode of about 1.9 m (including snow). As expected, level ice was prevalent but rough ice occupied almost 50% of fast ice volume, exceeding 6 m in ~10% of cases (Langhorne et al., 2023). The thicker fast ice was mostly observed along the northwestern Ross Sea and was often characterized by a layer of loose ice crystals beneath (up to 10 m) when in contact with floating glaciers.

### 3.3. Polynyas

Both SIE and SIT are strongly influenced by sea ice production in polynya areas that interconnect the atmosphere, ice, and ocean (Knuth and Cassano, 2014). Polynyas are highly dynamic stretches of open water and recently formed sea ice surrounded by a more extensive and thicker sea ice pack (Aulicino et al., 2018), which have been often deemed 'sea ice factories' (DuVivier et al., 2024), as they have large sea ice production rates, especially during autumn and winter seasons (Ohshima et al., 2016). They are generally classified as coastal (latent heat) and open ocean (sensible heat) polynyas (Smith et al., 1990; Martin, 2019; Lin et al., 2023). However, sometimes polynyas are a combination of the two types (Morales Maqueda et al., 2004) and several authors distinguish between mechanically driven and convectively forced polynyas (Williams et al., 2007).

Coastal polynyas are usually driven by cold and strong downslope winds that flow off the Antarctic continent and push sea ice away from the coast (Gordon and Comiso, 1988). Their action prevents newly formed frazil and pancake sea ice from consolidating as a thick pack and, at the same time, keeps the relatively warm open water surface exposed to a cold atmosphere, facilitating further sea ice formation (Budillon et al., 2000; Sansiviero et al., 2017). This mechanism is responsible for about 10% of the total Antarctic sea ice production that is then advected northward, advancing the sea ice edge (Tamura et al., 2008). Moreover, heat and salt released during frazil and pancake ice formation are essential for convection processes, dense water production and overturning processes modulation (e.g., Budillon and Spezie, 2000; Fusco et al., 2002; Tamura et al., 2016; Aulicino et al., 2019; Thompson et al., 2020; DuVivier et al., 2024).

Three coastal polynyas are known in the Ross Sea (Fig. 4): Ross Sea Polynya (RISP), McMurdo Sound Polynya (MSP) and Terra Nova Bay Polynya (TNBP), which are all considered important source regions of HSSW (Kern and Aliani, 2011; Farooq et al., 2023). The RISP, the largest Antarctic polynya with a winter area of about 20,000 km$^2$, is located along the northern edge of the RIS between Ross Island and the 180 meridian to the east (Burada et al., 2023) and presents the highest sea ice production rates among all Antarctic coastal polynyas (Nihashi et al., 2024). The MSP forms to the west of Ross Island, adjacent to fast ice on the coast next to the Transantarctic Mountains. Although the smallest of the three (about 900 km$^2$), it is a widely studied region because of its interactions with ice shelves and fast ice (Leonard et al., 2021; Farooq et al., 2023). The RISP and MSP normally occur simultaneously, as they are caused by strong Ross Air Stream events during which the southerly winds are split by Ross Island into a western and eastern airflow (Brett et al., 2020; Rack et al., 2021), and provide a consistent northward drift of sea ice away from the Ross Ice Shelf.

Recent studies suggest that the HSSW export from the RISP across the Drygalski Trough and the Glomar Challenger Trough are positively correlated with the meridional wind through variations in geostrophic ocean currents that result from sea surface elevation change and density differences (Wang et al., 2023). Mesoscale circulation in the Ross Sea has only recently been investigated (McGillicuddy et al., 2017) with the aim of highlighting how these aspects can represent a "noise" superimposed on the trends of interest that must be filtered out to obtain accurate estimates of such temporal changes (seasonal, annual, interannual, interdecadal, etc.). Wang et al. (2023) also studied the RISP response to synoptic-scale and mesoscale cyclones, showing that the former increases ice production by 20–30 % over the entire polynya, whilst the latter has a different response (increase/decrease) over the western/eastern RISP. HSSW production mainly occurs in the western RISP and persisted for 12–60 h after the decay of the cyclones under both case studies. Park et al. (2018) analyzed the trend of the RISP area over 1979–2014 and showed that it is significantly correlated with the ratio of the trend of the meridional to zonal wind components related to the Nino3.4 index.

The TNBP occurs north of the Drygalski Ice Tongue (DIT) and it is

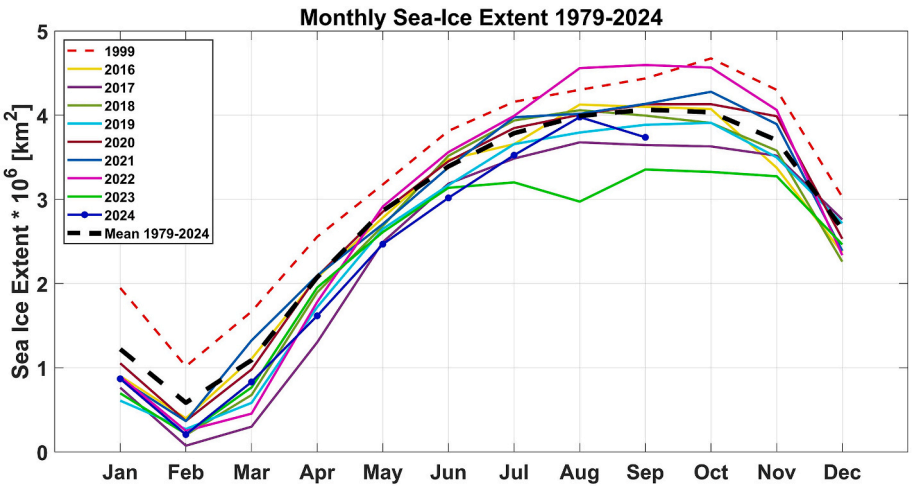


**Fig. 4.** Seasonal cycle of SIE in the Ross Sea since 2016. The black dashed line shows the 1979–2024 average extent; the red dashed line represents the year (1999) in which the maximum sea ice extent was observed. The SIE dataset is accessed through the sea ice index repository provided by NSIDC.

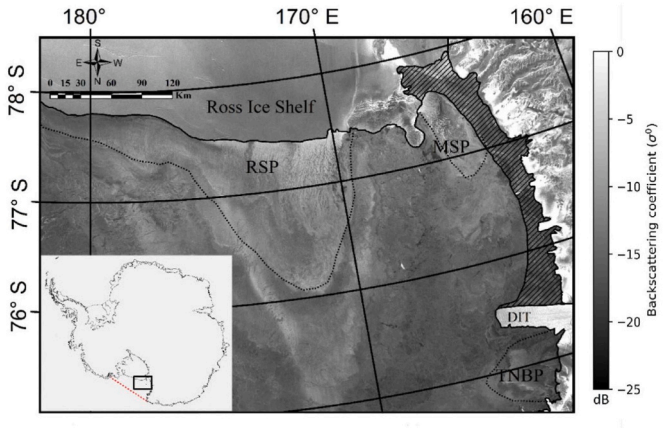


**Fig. 5.** The Ross Sea and the typical extent of its prominent polynyas (Ross Ice Shelf Polynya - RISP, McMurdo Sound Polynya - MSP and Terra Nova Bay Polynya - TNBP) as seen from the Envisat SAR image acquired on 16 June 2011 (Adapted from Farooq et al., 2023).

bordered by the Nansen Ice Sheet and the Campbell Ice Tongue (Inserra et al., 2024). The DIT serves to control the polynya size, as it acts as a barrier for the pack ice advected from the south and south-west (Kurtz and Bromwich, 1983), allowing the polynya to form and to be maintained (Fusco et al., 2009; Ciappa et al., 2012; Ciappa and Budillon, 2012). The TNBP opening is forced by katabatic winds, which reach the coast from the East Antarctic plateau and are channeled through the valleys of the Transantarctic Mountains (Van Woert, 1999; Thompson et al., 2020; Guest, 2021). The polynya area is characterized by large turbulent heat fluxes from the surface to the atmosphere (up to 2500 W $m^{-2}$; Ackley et al., 2021) and a high interannual variability with an opening/closing fluctuation depending on the regime of the katabatic winds (Aulicino et al., 2018). Katabatic winds account for about 45% of the days when the TNBP exceeded its mean extent plus one standard deviation (Fonseca et al., 2023). The negative phase of the SAM acts as the main driver of its expansion in the remaining days, especially during the transition seasons, when such events are more likely to reach Antarctica (Fonseca et al., 2023). Nevertheless, Lin et al. (2023) demonstrated that thick ice transiting, driven by large-scale winds transporting more sea ice to the outlet zone, affects the evolution and variation of the TNBP extent by blocking the newly-formed sea ice from leaving the bay.

To date, no significant trends can be observed in the variability of the three polynyas over the satellite era. However, Himmich et al., 2023 applied the Community Earth System Model version-2 (CESM2, Danabasoglu et al., 2020) to suggest a decline in RISP frequency in the future. This decline will likely be driven by wind speed decreases, due to large-scale atmospheric circulation changes related to the ASL variability, that hinder sea ice offshore advection, and by local positive feedbacks that would further decrease near-surface wind speed and increase sea ice cover. If such a decline in winter polynya frequency occurs over this century, it may strongly impact AABW formation, with dramatic consequences at local, regional and global scales.

## 4. The Ross Ice Shelf

The Ross Sea hosts the largest ice shelf in the world; with an area of ~480.000 $km^2$, the Ross Ice Shelf (RIS) is a floating extension of the grounded ice sheet and plays an important role in stabilizing the WAIS (Thomas and Bentley, 1978) and limiting its contribution to the sea level rise. It controls the loss of grounded ice from Antarctica through a process called “buttressing”, imparting stress on the upstream grounded ice and slowing its flow into the ocean (Das et al., 2020; Paolo et al., 2015). The RIS thickness ranges from 200 to 400 m along the ice front to nearly 1000 m at the Siple Coast grounding line (Griggs and Bamber, 2011), and although it is currently considered to be stable, geological records suggest that it may be undergo rapid disintegration (Tinto et al., 2019). Sediment core records indicate that the RIS collapsed and experienced a significant retreat (of about 280,000 $km^2$) approximately 5000 years ago as a result of atmospheric warming combined with warm ocean currents impacting the continental shelf (Yokoyama et al., 2016). Were the RIS to completely disappear (as foreseen after 2100 AD in a warming subsurface Southern Ocean temperature scenario yielding an increase of basal melting), it would result in a sea level rise of 0.5 m (Park et al., 2023). In addition, the potential thinning of the ice shelf can reduce the buttressing effect on the grounded ice, leading to an increasing ice discharge into the ocean. Tinto et al. (2019) emphasize that the RIS is formed from two catchments, with a cumulative sea level rise potential of 11.6 m (2.0 from the WAIS, 9.6 from the EAIS), highlighting the importance of the RIS in restraining the Antarctic Ice Sheet mass loss, and the need to understand its dynamics and its long-term stability in a changing climate.

The ice shelf buttressing loss occurs via iceberg calving and basal melt. The East Antarctic side of the Ross Ice Shelf loses mass equally through basal melting and calving, while mass loss on the West Antarctic side is dominated by calving (Rignot et al., 2013). Generally, the iceberg calving is the primary driver of buttressing losses for a large and

cold-cavity ice shelf like the RIS (Rignot et al., 2019). The difference between cold cavity and warm cavity ice shelves depends on whether the dominant process causing basal melting is the inflow of cold HSSW or warmer CDW (Nelson et al., 2017). Indeed, cold-cavity ice shelves with areas >100,000 $km^2$, such as Ross and Filchner - Ronne Ice Shelf, are in contact at their base with water mass close to the surface freezing point (~- 1.9 °C) (Vaňková et al., 2021) which limit their exposure to CDW. Basal melting thus depends on the ocean circulation along the ice front and underneath the ice shelf. Jacobs et al. (1992) identified three modes of sub-ice shelf circulation (Fig. 6) based on water masses driving melt. Mode 1 circulation occurs when HSSW flows beneath the ice shelf due to the inland-deepening sea bed. Melting of the RIS draft and cooling due to the contact with the ice determine the formation of ISW. This circulation mode is considered to be responsible for melting processes beneath the Filchner-Ronne, Amery and Ross Ice Shelves. The second circulation (Mode 2) involves warm inflows from the slope-front region of CDW, a relatively warm water mass which can cross the shelf and access ice shelf cavities, driving rapid melting throughout the cavity, as observed at Pine Island Glacier (Jenkins et al., 2010). The last mode of circulation (Mode 3) derives from intrusions of summer-warmed AASW into the frontal region of the cavity, where tidal pumping and coastal currents are thought to bring this water mass in contact with the ice base (Jacobs et al., 1992).

The Ross Ice Shelf is the most studied portion of the Antarctic ice sheet (Thomas and MacAyeal, 1982) and the first with geological and oceanographic observations (performed in a single borehole through the central shelf) providing measurements of ice thickness and velocity, strain rates, bottom depth, snow accumulation, mean annual temperature, and topography of the sea floor (Clough and Hansen, 1979). The first measurements of melting beneath the ice shelf and the sub-ice shelf circulation were obtained after 1978, when a net melting at the ice shelf base was observed, together with an inflow of seawater beneath the ice shelf from a central warm core and from HSSW, which flows beneath the western sector of the ice shelf (Fig. 7). Initial long-term observations near the Ross Ice Shelf detected mCDW entering the cavity near 172° W, inducing considerable basal melting; this water mass was considered a primary heat source for melting of the ice shelf (Pillsbury and Jacobs, 1985). Instead, it is now believed that mCDW is recirculated near the ice front (Smethie and Jacobs, 2005), and that RIS basal melting is primarily driven by the seasonal inflow of summer-warmed water that melts ice along the ice shelf front, and by the inflow of cold HSSW that melts ice near the grounding lines (Assmann et al., 2003; Stewart et al., 2019; Tinto et al., 2019; Baldacchino et al., 2022). Temperature and current data from a mooring placed provided first year-round evidence of ISW formation below the RIS (Bergamasco et al., 2002). Holland et al. (2003) modeled the HSSW inflow along the sea floor in the cavity and mode 1 circulation. This ISW outflow was directly observed between Ross Island and Coulman High by an autonomous glider traveling beneath the ice shelf front (Nelson et al., 2017) and during oceanographic cruises carried out along the RIS front.

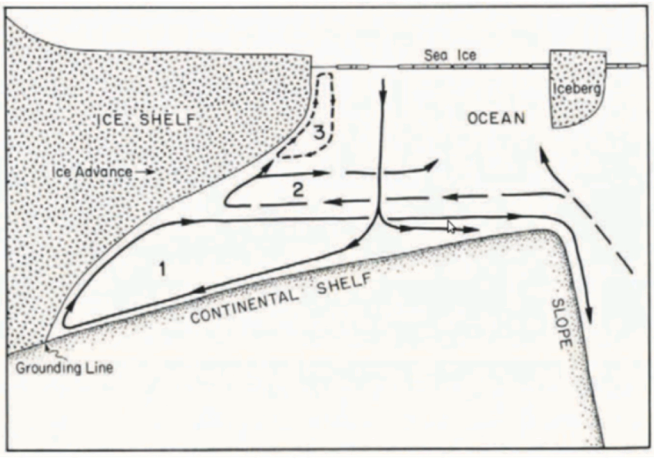


**Fig. 6.** Modes of sub-ice shelf circulation proposed by Jacobs et al. (1992).

Recent works on sub-ice shelf circulation have been focused on the inflow of seasonally warmed AASW into the RIS cavity and the role of this water mass in driving basal melting (Stewart et al., 2019; Tinto et al., 2019; Das et al., 2020). The intrusion of AASW into the cavity is believed to be driven by a combination of processes such as tides (Arzeno et al., 2014), eddies (Li et al., 2017), and isopycnal deepening under a freshwater wedge along the ice front (Malyarenko et al., 2019). Basal melting estimates suggested that AASW inflow causes melting close to the ice shelf and contributes substantially to the basal mass balance of the RIS (Stewart et al., 2019). Bathymetric data combined with model simulations provided insights about RIS basal melting (Tinto et al., 2019) driven by AASW and HSSW inflow and interaction with the ice shelf (Fig. 7). HSSW flows under the ice front near Ross Island and moves southward along the base of the Transantarctic Mountains without crossing the tectonic boundary (dotted line, Fig. 7) towards the West Antarctic side. Instead, it exits the ice shelf cavity moving northward.

Results from observations and models suggest that the sub-ice-shelf circulation and variability drive the basal melting rate near the ice front (Arzeno et al., 2014), and that the sensitivity to basal melting is spatially and seasonally variable (Baldacchino et al., 2022; Tinto et al., 2019; Holland et al., 2003, Assmann et al., 2003). While basal melt rates averaged over the entire ice shelf remain low (ca. 0.1 m $yr^{-1}$; Rignot et al., 2013; Reese et al., 2018; Das et al., 2020), near the ice front east of Ross Island, higher basal melt rates have been estimated (Tinto et al., 2019; Arzeno et al., 2014; Dinniman et al., 2018; Das et al., 2020), together with the largest rates associated with AASW intrusion in summer season (Stewart et al., 2019; Malyarenko et al., 2019).

Sub-ice shelf circulation influences basal melting beneath the ice shelf, which in turn affects the future stability of the RIS (Stewart et al., 2019). These findings highlight the need to further investigate sub-ice shelf circulation and ice shelf response to local climate processes that can influence its basal melting and stability in the future.

## 5. Hydrography and dynamics

### 5.1. Main water masses

The surface layer of the Ross Sea is occupied by the Antarctic Surface Water (AASW), typically fresh and with temperatures depending on the season and latitude. Underneath, the layer between the AASW and the SW is broadly occupied by modified Circumpolar Deep Water (mCDW), the only water mass that is not entirely of local origin. It is formed by the cooling of Circumpolar Deep Water (CDW), the most abundant water mass transported by the Antarctic Circumpolar Current (ACC), and by its mixing with AASW and SW. CDWs consist of two water masses, Upper CDWs (UCDW) characterized by an oxygen minimum, and Lower CDWs (LCDW) that are recognizable by a relatively high salinity (Orsi et al., 1995).

The main shelf waters (SW) forming on the continental shelf are the High Salinity Shelf Water (HSSW), the Ice Shelf Water (ISW), both precursors of the AABW, and the Low Salinity Shelf Water (LSSW). Orsi and Wiederwohl (2009) described the characteristics of the shelf waters in terms of potential temperature, practical salinity, neutral density and the areas and vertical layers occupied by these water masses. The shelf waters generally fill the deepest layer of the continental shelf.

HSSW and ISW both contribute to the formation of the AABW by entrainment of LCDW along the continental slope (see next section). The CDW enters onto the shelf mainly through the western side, crossing the shelf break and carrying heat and nutrients onto the shelf and becoming mCDW. The ranges of potential and conservative temperature, of practical and absolute salinity as well as of neutral density of the main Ross

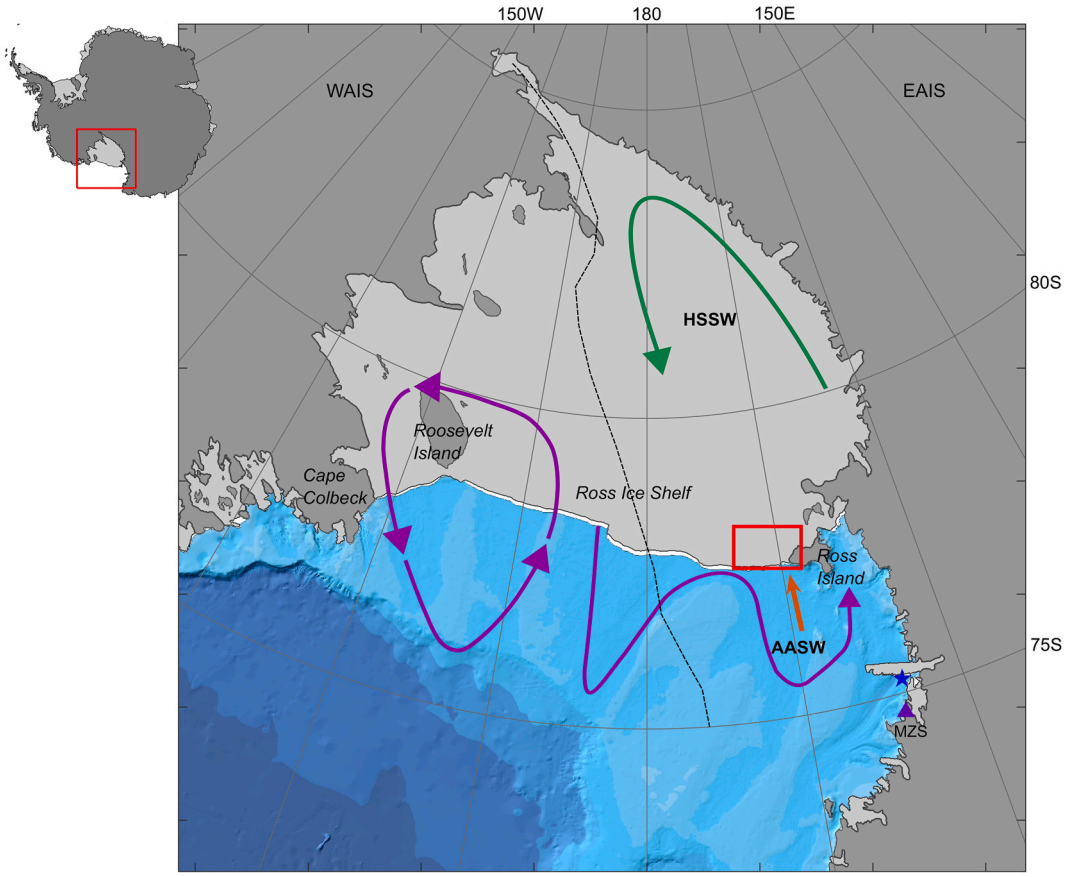


**Fig. 7.** Schematic of processing controlling the Ross Ice Shelf adapted from Tinto et al. (2019). Red box represents the area with high basal melt rates according to Stewart et al. (2019). Blue star indicates the deployment position of the Argo float in Terra Nova Bay in 2021. In purple, sub-surface circulation following Locarnini (1994). Dotted line: tectonic boundary in the manner of Tinto et al. (2019) (Fig. 5). AASW: Antarctic Surface water; HSSW: High Salinity Shelf Water; EAIS: East Antarctic Ice Sheet; WAIS: West Antarctic Ice Sheet; MZS: Mario Zucchelli Station. The map and bathymetry of the Ross Sea is based on IBCSO (Arndt et al., 2013; Greene et al., 2017).

**Table 1**
Temperature and salinity ranges of the main Ross Sea water masses. Practical salinity and potential temperature from Orsi and Wiederwohl (2009).

| Water Mass | Neutral Density (kg $m^{-3}$) | Practical Salinity | Absolute Salinity* (g $kg^{-1}$) | Potential Temperature (°C) | Conservative Temperature* (°C) |
|---|---|---|---|---|---|
| AASW | $\gamma^n <$ 28.00 | S < 34.30 | $S_A <$ 34.4658 | θ > -1.85 | $C_T > -1.8467$ |
| SW | $\gamma^n >$ 28.27 | | | θ < -1.85 | |
| CDW | 28.00 $<\gamma^n<$ 28.27 | | 34.79$<S_A$ < 34.92 | | 1.2$<C_T <$ 1.6 |
| mCDW | 28.00 $<\gamma^n<$ 28.27 | | | | |
| ISW | $\gamma^n >$ 28.27 | | | θ < -1.95 | $C_T < -1.9469$ |
| LSSW | $\gamma^n >$ 28.27 | S < 34.62 | $S_A <$ 34.7874 | θ < -1.85 | $C_T < -1.8469$ |
| HSSW | $\gamma^n >$ 28.27 | S > 34.62 | $S_A >$ 34.7874 | θ < -1.85 | $C_T > -1.8469$ |
| AABW | $\gamma^n >$ 28.27 | | | θ > -1.85 | $C_T > -1.8471$ |

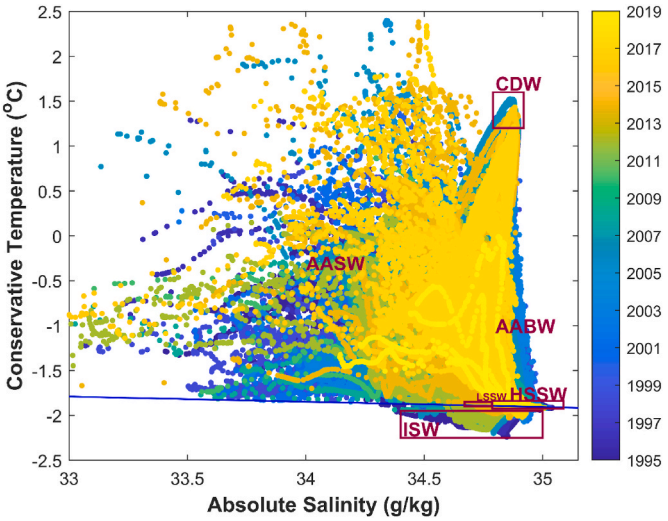


**Fig. 8.** Conservative temperature-absolute salinity diagram of all CTD casts made from 1995 to 2019 by PNRA oceanographic cruises in the Ross Sea. Water masses and ranges are reported over the diagram.

Sea water masses are well known (Table 1, Fig. 8).

### 5.2. Water mass formation

HSSW forms in the mechanically driven polynya of TNB (Fig. 1). Due to the strong katabatic winds and air-sea interactions, to the Drygalski Ice Tongue that prevents sea ice lateral advection and eventually, to brine rejection with sea ice formation, the water column of TNB increases its salinity and decreases its temperature to the surface freezing point. The period of HSSW formation spans from May to October and a homogenous layer of conservative temperature ∽ −1.92 °C and absolute salinity ≥34,92 g $kg^{-1}$ fills the entire water column (Fig. 9). Convection, at a rate ranging from 0.5 to 1 m $h^{-1}$, carries transformed surface waters to depth, whereas the deepest layer is already occupied by HSSW formed the previous year. A net production of 0.4 Sv was estimated (Morales Maqueda et al., 2004; Rusciano et al., 2013; Miller et al., 2024).

HSSW is also produced in the RIS polynya area (Orsi and Wiederwohl, 2009). Recent observations (Falco et al., 2024) estimated a production from 0.1 to 0.4 Sv, depending on the polynya area considered. ISW forms in the cavity of the RIS through a transformation process of HSSW. HSSW is transported under the cavity along the seafloor; at the grounding line, due to pressure effects, it carries a large amount of heat to melt the RIS base. The meltwater decreases the salinity of the HSSW but also its temperature. The overall effect on density is a decrease; thus the resulting water is fresher, colder and more buoyant, and rises along the RIS. As the depth decreases, the freezing point increases and the water in contact with the RIS refreezes. The newly formed ISW reaches a neutral buoyancy depth and eventually exits the cavity at about 400 m, offsetting the previous inflow of HSSW.

According to Orsi and Wiederwohl (2009) the LSSW has a volume much lower than the HSSW. It is more abundant on the inner eastern continental shelf, which can be considered as its source region, and is formed by the release of salt as sea ice forms and by the resulting loss of buoyancy of the surface layer of AASW. On the other hand, the minimal temperature and salinity differences between LSSW and SW of the central-eastern sector of the Ross Sea provide another mechanism for the formation of LSSW, i.e., LSSW can be derived from SW (at temperatures of about −1.9 °C) that has undergone a slight salinity increase (Orsi and Wiederwohl, 2009). There is then a salinity gradient between the

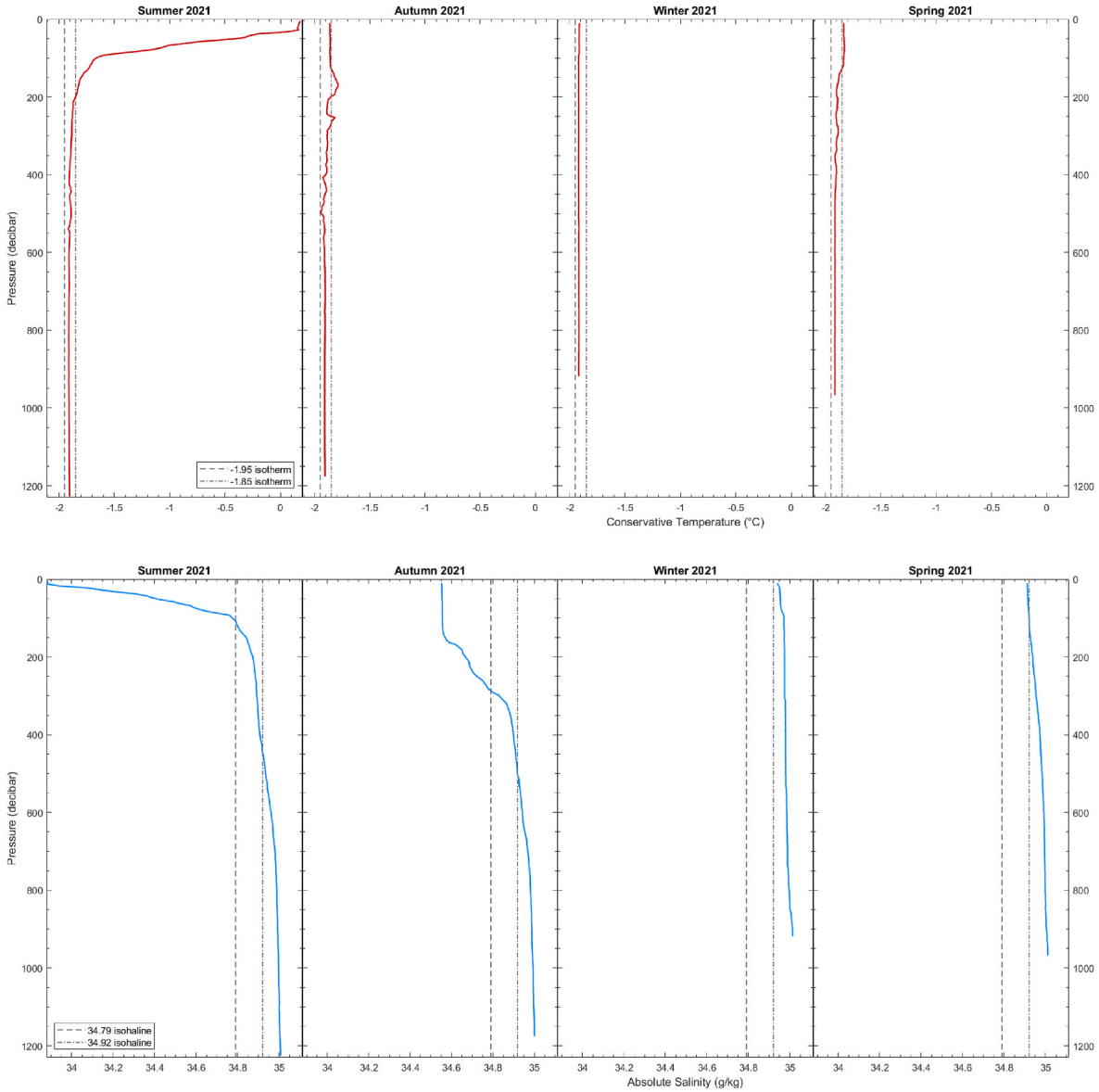


**Fig. 9.** Absolute Temperature (from a to d) and absolute salinity (from e to h) profiles collected by an Argo float in TNB polynya area during 2021. The profile of Winter and Spring are shallower because the float moved over a shallower area (Fig. 7).

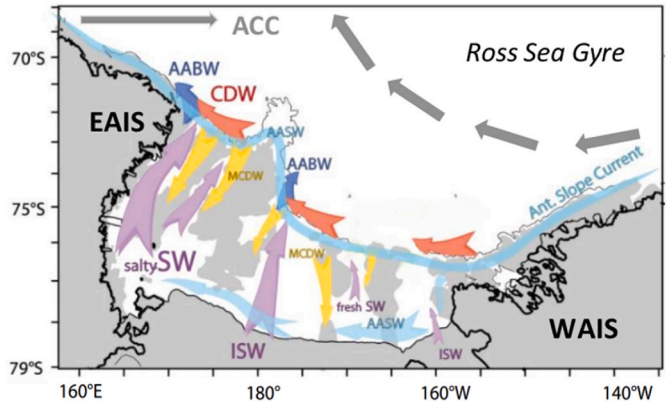


**Fig. 10.** Averaged circulation of Ross Sea water mass. Colors represent individual water masses. AASW: light blue. HSSW (SW in figure): purple. mCDWater (mCDW): orange. CDW: red. AABW: dark blue (Adapted from Fig. 3; Smith et al., 2012).

western and eastern sectors due to the polynya activities and HSSW formation in the west. ISW flowing from the RIS cavity in the east (Fig. 10) shows a lower salinity than the ISW formed from HSSW transformation.

The meridional circulation of the Southern Ocean transports relatively warm and saline LCDW from the ACC to subsurface layers near the Antarctic shelf break. In the Pacific sector, the connection between the ACC and the coast is accomplished by the Ross Gyre; thus, LCDW flows cyclonically in the gyre to lap the Antarctic continental margin. The largest volume of LCDW (~1500 m thick which becomes thinner as it approaches the shelf break) is found offshore of the 700-m isobath. mCDW is formed near the shelf break from the mixture of the relatively fresh and cold AASW with the salt and low-oxygen LCDW below (Orsi and Wiederwohl, 2009). Temperature and salinity values of mCDW change over the continental shelf as a function of the degree of mixing and local influences. mCDW also carries nutrients and micronutrients onto the continental shelf, promoting primary productivity, especially in the western sector (Rivaro et al., 2020).

### 5.3. Circulation of water masses

The ACC, which transits around Antarctica and extends from the surface to a depth of about 2 km, does not influence the Ross Sea directly but is mediated by the Ross Gyre. The southwestern branch of the gyre results in an intense current that moves westward near the continental slope and plays a crucial role in the exchange of the relatively warm ACC water masses with the cold DSW of the continental shelf. The CDW enters the eastern limit of the Ross Gyre, moving first southwards and then westwards following the outer limit of the continental slope. Subsequently, the CDW enters the Ross Sea continental shelf at locations where the bottom topography changes direction relative to the slope flow (Klinck and Dinniman, 2010). Aided by tidal advection, it then moves across the shelf break (Whitworth and Orsi, 2006; Padman et al., 2009; Castagno et al., 2017) and is transported by barotropic flow southward, mainly on the west slope of the Ross Sea banks (Kohut et al., 2013). However, Castagno et al. (2017) found the presence of two main cores of CDW that intrude over the shelf in the Drygalski Trough.

Using a time series of hydrographic and current observations close to the shelf break, Castagno et al. (2017) showed the seasonal and interannual variability of the CDW intrusion across the continental shelf. A strong inflow occurs each year around late December and early January, while a weaker inflow is observed in July. They observed a strong relationship between tides and temperature from daily to seasonal time scales and concluded that the seasonality of CDW inflow is strongly modulated by the semi-annual tides, with a strong CDW inflow near the December solstice. During the measurements, they also found a shift in the CDW intrusion around 2010, accompanied by significant differences in temperature. They attributed this change to the influence of stratification on the diurnal, topographically trapped vorticity waves (DTVWs). In the northwestern Ross Sea, tidal currents are associated with the DTVWs (Robertson, 2005; Padman et al., 2009), with their propagation and attenuation rates varying based on the stratification. A more homogenous water column post-2010 reduced the tidal influence. These all suggest that the cross-shelf exchange between the AABW and the CDW over the continental shelf at different time scales is significantly influenced by the tides.

CDW intrudes onto the Ross Sea continental shelf and mixes with DSW and the slope front waters to form modified Circumpolar Deep Water (mCDW). The mCDW has been found in TNB subsurface layer (Rusciano et al., 2013). The Antarctic slope front is a large cross-slope density gradient, associated with the Antarctic Slope Current (ASC). The ASC, driven primarily by winds and buoyancy forcing, is a westward flow that encircles the Antarctic continental shelf (Thompson et al., 2018). In the southeast Pacific sector of the Southern Ocean, the ASC advects AASW from the Amundsen Sea into the Ross Sea. At the eastern gate of the Ross Sea near Cape Colbeck, the ASC splits into a narrow coastal current that flows westward along the Ross Ice Shelf and the slope current that moves along the shelf-break toward west (Smith et al., 2012). Both the coastal current and the ASC import freshwater from the Amundsen Sea into the Ross Sea, contributing to the Ross Sea salt budget and influencing the DSW salinity formation and variability (Castagno et al., 2019; Jacobs et al., 2022).

The HSSW formed in TNB sinks and moves along the bottom following the Drygalski trough towards north-east and south-east (purple arrows in Fig. 10). The part that flows in a north-easterly direction reaches the edge of the continental shelf and participates in the formation of the saltine, warm type of AABW (Jacobs et al., 1970; Whitworth and Orsi, 2006; Capello et al., 2009; Rivaro et al., 2010; Budillon et al., 2011). The HSSW that runs south-eastward forks north of Ross Island into a branch that flows eastwards and occupies the entire seafloor to about 175°E, where it is blocked by the eastern side of Ross Bank (Budillon et al., 2003). The other branch moves southwards, wedges under the Ross Ice Shelf and contributes to the formation of the ISW (Jacobs et al., 1970, 1979, Jacobs and Fairbanks, 1985; Jacobs and Giulivi, 2010; Jacobs and Comiso, 1989; Trumbore et al., 1991; Budillon et al., 2003), together with the HSSW produced in the RIS polynya (Orsi and Wiederwohl, 2009).

At about 180°, the ISW flows from under the RIS and moves northwards through the Glomar Challenger Trough (GCT) (Bergamasco et al., 2002; Budillon et al., 2003, 2006; Orsi and Wiederwohl, 2009) and reaches the shelf break at about 75°S, where it mixes with the mCDW and contributes to the formation of the less dense AABW (Jacobs and Fairbanks, 1985; Trumbore et al., 1991; Budillon et al., 2011). AABW production and export from the western Ross Sea shows both seasonal and interannual variability (Gordon et al., 2015; Castagno et al., 2017). Tidal mixing and advection play critical roles in this variability (Whitworth and Orsi, 2006; Muench et al., 2009; Padman et al., 2009; Budillon et al., 2011; Castagno et al., 2017; Bowen et al., 2021, 2023). Bowen et al. (2021), showed that the dense water pulses from the continental shelf occur every year around the equinoxes. Bowen et al. (2023) observed that the strongest and densest outflow occurs when the salinity in Terra Nova Bay is high and the tides are weakest during a minor lunar standstill. The weakest outflow occurs near a major lunar standstill when tides are strongest. They also observed that flows and temperatures in the Drygalski Through vary significantly with the tides. The monthly-averaged outflow increases when the tidal flow decreases during the equinoxes and is highest during the solstices. During the maximum tidal currents, the mCDW is mixed to the bottom (Castagno et al., 2017). Bowen et al. (2023) concluded that the flow and density of bottom water leaving the western Ross Sea is a balance between the density in Terra Nova Bay, which drives the outflow, and the bottom

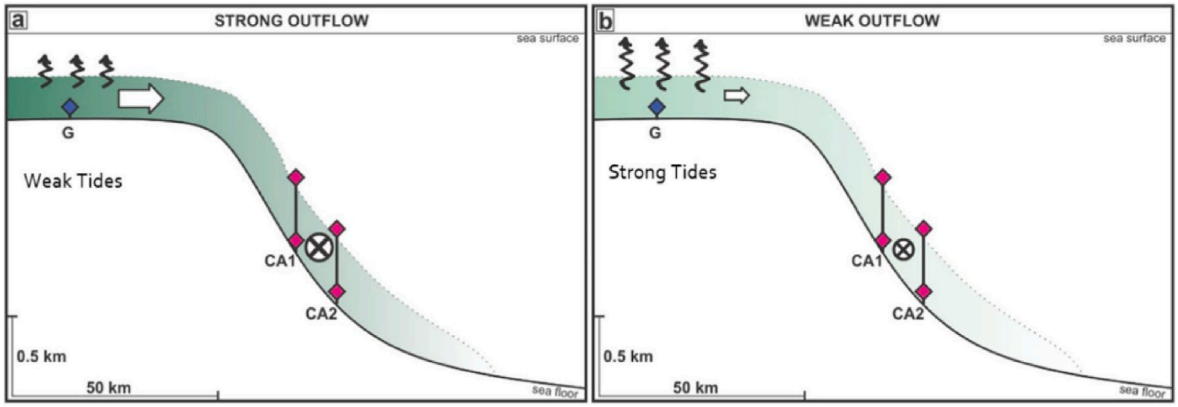


**Fig. 11.** The link between outflow, tides and density in Terra Nova Bay. The flow out of the trough (white arrows) turns to the left and flows along the slope past the moorings (flow is into the page in the diagram and indicated by the circle with a cross). The strength of the outflow depends on the tidal mixing in the trough (curly arrows) and on the density of the bottom water from Terra Nova Bay (shown by the green shading where darker green indicates denser water). (a) A stronger outflow of more dense water results when tides are weaker and water in Terra Nova Bay has a higher density. (b) A weaker outflow of less dense water results when tides are stronger and water in Terra Nova Bay is less dense. (From Bowen et al., 2023).

stress due to the tides in the trough, which slow the flow (Fig. 11). Weaker tides reduce bottom stress and allow the release of dense water from DT.

Winds have also been suggested as a driving force behind the release of dense water from the Drygalski Trough by shifting the density fronts at its mouth (Gordon et al., 2015). The dense water outflow from the continental shelf occurs as a 300–400 m thick gravity current over the continental slope (Budillon et al., 2002, 2011; Gordon et al., 2009; Visbeck and Thurnherr, 2009), moving as a geostrophic flow and leaving the Ross Sea between the 1500 and 2000 m off Cape Adare (Gordon et al., 2015).

### 5.4. Dense shelf water salinity variability

Over 60 years of hydrographic observations in the Ross Sea have shown a nearly linear decrease in salinity at 500 m near Ross Island of $-0.027$ decade$^{-1}$ from 1956 to 1957 to 2019–2020 and of $-0.029$ decade$^{-1}$ in the deep layer in TNB from 1959 to 2018 (Jacobs et al., 2022). Castagno et al. (2019) observed a strong rebound in salinity at 4 different locations in the western Ross Sea (including TNB and Ross Island) from 2014 to 2018 to values last observed in the mid-to late 1990s. The increase in salinity was large and rapid compared to the trend observed before 2014. Castagno et al. (2019) observed interannual variability superimposed on the overall negative salinity trend. At all sites, strong fluctuations in salinity are observed throughout the water column with a time scale of 5–10 years. Jacobs et al. (2022) hypothesized that the 60-year freshening of the Ross Sea is caused by the increase in glacial melt upstream of the Ross Sea in the Amundsen and Bellingshausen Seas (Rignot et al., 2013; Rignot et al., 2019; Adusumilli et al., 2020; Smith et al., 2020), which is advected by the westward-flowing coastal current towards the Ross Sea.

The rapid increase in DSW salinity after 2014 was attributed by Silvano et al. (2020) to increased sea ice formation throughout the Ross Sea, driven by the weakened easterlies associated with a strong El Nino and a positive SAM. During the 2015–2018 period, an anomalous positive SAM and a negative SOI occurred. This superposition caused a weakened ASL that in turn led to westerly anomalies along the coast in the Amundsen Sea. Weakened easterly winds reduced sea ice import from West Antarctica into the Ross Sea. The lower sea ice import led to a lower sea ice concentration over the Ross Sea continental shelf at the end of the summer. As a result, there was more open water at the beginning of winter, a condition that favored sea ice formation and caused a greater release of brine and a more saline Ross Sea DSW formed on the continental shelf. Guo et al. (2020) also hypothesized that the ASL variability modulates the formation of DSW salinity in the Ross Sea. After 2013, they observed a southwestward shift of the ASL, which led to an eastward anomaly of the coastal current and consequently to a reduction of freshwater input to the Ross Sea along the coastal current from the Amundsen Sea.

## 6. Modeling studies

Ocean modeling plays an important role in providing a theoretical understanding through hindcasting and forecasting in complex areas as the Ross Sea, where interactions occur among atmosphere, ocean and cryosphere. Dinniman et al. (2003) have analyzed the transport of warm, nutrient-rich CDW on the Antarctic continental shelf and the effects on dynamics in the Ross Sea with a high-resolution model based on the Regional Ocean Modeling System (ROMS). The circulation was found to be strongly influenced by the bottom topography due to weak stratification, and a significant correlation was found between the curvature of the shelf break and the transport through it. The balance of momentum terms shows that momentum advection contributes to forcing flow through the shelf break at specific locations due to the curvature of the bathymetry. For the model to create a strong CDW intrusion on the platform, two mechanisms appear to be required. First, the CDW is pushed onto the platform at least in part due to momentum advection and curvature of the platform break; then, the general circulation on the platform carries the CDW inward. Dinniman et al. (2007) also investigated the effects of changes in sea ice on the circulation and distribution of water mass, including the cavity beneath the RIS. Sea ice concentrations were specified from satellite observations, so that the effects of changes in sea ice due to iceberg C-19 could be examined. The heat budget around the RISP showed that the dominant term in the surface heat budget is a net exchange with the atmosphere, but oceanic warm water advection is also important. More recently, regional circulation models for the West Antarctic Peninsula and the Ross Sea were used to examine the dynamics of CDW intrusions onto the continental shelf (Dinniman et al., 2011). The CDW intrudes onto the shelf at specific points determined by the bathymetry, with a significant correlation with wind stress; the intrusions are at least partly related to short-duration wind events. The mixing of the CDW with surface waters of the Ross Sea was found to be more vigorous, especially to the west, where the HSSW is formed.

The circulation in the sub-ice shelf cavity beneath the RIS and the melting and freezing regimes at the base of the ice shelf have been investigated with a modified version of the Miami isopycnic coordinate OGCM (Holland et al., 2003). The pathways of waters entering and

exiting the cavity were analyzed through a Lagrangian technique and the model results were compared with data collected both in the cavity and along the ice shelf front. HSSW flows into the cavity and is transformed into the ISW upon contact with the ice shelf base. Rapid melting is driven by the ventilation of the region near the ice shelf front, which is in turn forced by seasonal variations of the water column density. Net melting over the entire ice shelf base is lower than previous estimates, but the simulated estimate may increase if additional forcings are added to the model.

Currents and their seasonal variability over the Ross Sea continental shelf have been investigated - with a focus on density-driven winter intensification - using a climatological ocean-ice shelf coupled model of the Ross Sea (Jendersie et al., 2018). The model included the cavity and prescribed sea ice fluxes. Two persistent cyclonic and three anticyclonic circulation features were identified. The seasonal variability was found to be basically driven by the baroclinic pressure gradients associated with lateral differences in density, while winds were found to play a minor role in the variability. On the other hand, the source of momentum in the cavity was due to the gravity-driven bottom flow of HSSW, which is in turn produced in the Ross Sea Polynya.

Understanding the ocean–atmosphere–sea ice interactions is fundamental to predict Southern Ocean and Antarctic continent future scenarios. As such, regional coupled climate–sea ice–ocean models are needed for polar regions. Several such models have been developed; however, the conservation of heat and mass fluxes between coupled models is often overlooked. At a regional scale, the non-conservation of water and energy can lead to model drift in long-term simulations. In the coupled Polar Scripps-KAUST PWRF-MITgcm model for the Ross Sea region, Malyarenko et al. (2023) included a full conservation of heat and mass fluxes transferred between the climate and sea ice–ocean models. Open water, sea ice cover, and ice sheet interfaces were examined. Evidence of the flux conservation in the results of a 1-month-long summer and 1-month-long winter test experiment showed the implications of conserving heat flux over the TNB and Ross Sea polynyas in August 2016. In summary, conservation of heat and mass is shown to be possible over long-term simulations, as requested for reliable future projections. Such coupled model setup is therefore recommended for climate modelling in any Arctic and Antarctic region.

Modeling studies specifically aimed at analyzing the Ross Sea circulation and its forced and intrinsic variability during the ice-free period are lacking. In this regard, the Parthenope Southern Ocean Model (PARSOM; A. Colella, P. de Ruggiero, S. Pierini, personal communication) analyzes the summer months of an ensemble of numerous simulations, each lasting ten years (2010–2020). The model focuses on the Ross Sea but includes the entire Southern Ocean, so that no spurious lateral boundaries affect the internal response. The PARSOM SSH summer average compares well with the SSH 2013–2018 annual average (Fig. 12) obtained by Prend et al. (2024) using the data-assimilating Biogeochemical Southern Ocean State Estimate (Verdy and Mazloff, 2017).

One of the main results of PARSOM, which evolves freely without any constraint (apart from the relaxation to climatology implemented in the model), concerns the interpretation of the Ross Gyre variability. The cyclonic circulation of the gyre is clearly due to the input of negative vorticity provided by the surface wind field; however, the Ross Gyre variability cannot be explained by similar changes in atmospheric forcing. On the other hand, the analysis of the sea surface height and of the barotropic streamfunction highlights a see-saw behavior between the core of the Ross Gyre and its northern and eastern flanks. Consequently, such variability is clearly driven by the low-frequency fluctuations of the ACC, which are fundamentally chaotic due to intrinsic nonlinear oceanic mechanisms associated with the mesoscale eddy field (e.g., Carret et al., 2021; Hogg et al., 2022). This suggests that, despite the quasi-linear character of the Ross Gyre circulation, its low-frequency changes may be chaotic in nature and therefore unpredictable beyond a limited time.

All these model studies rely on realistic implementations. However, it is also worth considering simpler model implementations; these can be valuable tools to investigate basic dynamical aspects that might otherwise be overshadowed by the more complex outputs of realistic implementations. Commodari and Pierini (1999) applied a barotropic primitive equation model to a realistic Ross Sea to study the vertically integrated transport induced both by local winds and by the external action of the East Wind Drift during the ice-free season, providing valuable insights into the respective role of the local and remote forcing in shaping the circulation. The remote effect of the boundary forcing given by the ACC and the EWD in the absence of local winds was found to be notably weaker than the locally forced flow.

In a relatively idealized context, Rubino et al. (2003) applied a nonlinear, reduced gravity, layered numerical model to simulate the process of spreading and sinking of the Deep Ice Shelf Water (DISW) in the Ross Sea. In the most realistic simulation, the path and density structure of the DISW vein flowing over the Challenger Basin were found to be in good agreement with data. The evolution of the DISW layer beyond the continental shelf was also investigated; the results were useful in a region where the paucity of data does not allow for a detailed description of the deep ocean dynamics.

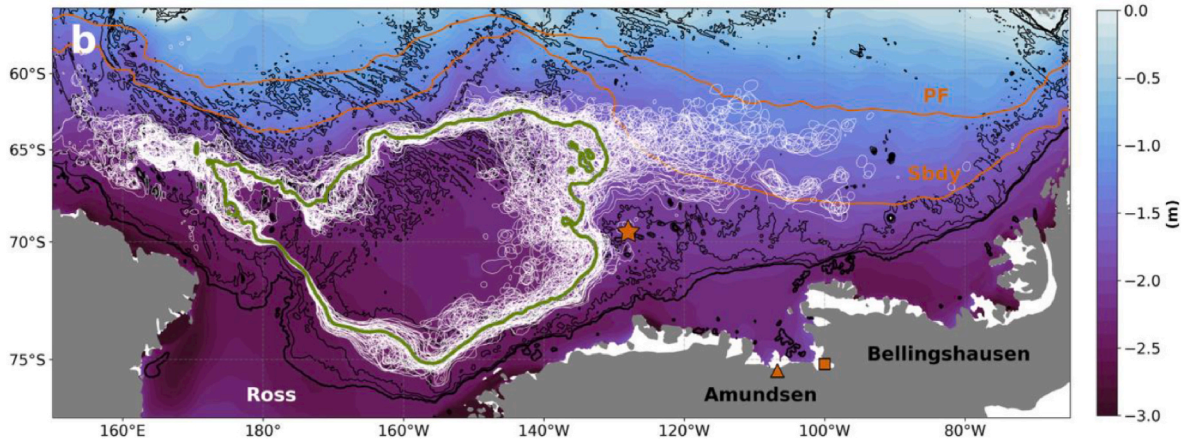


**Fig. 12.** SSH averaged over the years 2013–2018 obtained by Prend et al. (2024) using the data-assimilating Biogeochemical Southern Ocean State Estimate (Verdy and Mazloff, 2017), which constrains the MITgcm solution (Marshall et al., 1997) with satellite and hydrographic measurements. Each white line represents a monthly mean of the −8 Sv contour of the barotropic streamfunction. The green line represents the −8 Sv contour of the barotropic streamfunction averaged over the entire period. The black lines show the bathymetry with 1000 m intervals; the 1000 m-isobath (thick line) shows the Antarctic Slope Front (from Prend et al., 2024).

## 7. Conclusions

The Ross Sea is one of the most studied areas of the Southern Ocean. It is a source of Antarctic Bottom Water (AABW) and dense water production occurs over large sectors of the continental shelf. However, a number of questions regarding its functioning remain. Through the early 2010s, AABW freshened, warmed, and contracted in volume (Purkey and Johnson, 2013). The strongest freshening is believed to be related to multidecadal decrease in salinity of the Ross Sea component of AABW that results of the intrusion of fresh water from the Amundsen and Bellingshausen Seas (Jacobs et al., 2022). The reasons for the warming are still unclear. Hypotheses include changes in the DSW properties (Purkey and Johnson, 2012, 2013), changes in the mixing ratio between DSW and CDW, and changes in the current field including a slowdown of the overturning circulation. The lack of observations around the Antarctic margin makes it difficult to identify the real causes and models are limited in predicting AABW changes in the future (Purich and England, 2021). As a result, a weakening of the abyssal overturning and ventilation in sectors of the Southern Ocean under the direct influences of the AABW formed at the Ross Sea shelf break were observed. A net slowdown of $-0.8 \pm 0.5$ Sv decade$^{-1}$ thinned the deepest layers of the Australian Antarctic Basin, driving deoxygenation of $-3 \pm 2$ μmol kg$^{-1}$ decade$^{-1}$ from 1994 to 2017 (Gunn et al., 2023).

Castagno et al. (2019) documented a rebound in salinity since 2014 and Aoki et al. (2020) noticed a reversal of the freshening trend of AABW in the Australian Antarctic Basin in the second half of the 2010s. They also pointed out that the source of the salinity reversal signal is located to the east of the Australian Antarctic Basin. Furthermore, they found a salinity increase rate very close to those reported in Castagno et al. (2019). However, there is no evidence of a new decrease of salinity in the Ross Sea DSW, whereas models predict volume contraction and warming of the AABW. Li et al. (2023) using a high-resolution coupled ocean–sea-ice model and assuming a high-emissions scenario suggest that the abyssal warming may increase over the next 30 years and contract that would allow for a larger intrusion of CDW onto the continental shelf.

The recent changes in the sea ice extent around Antarctica points out the urgency of improving our capability to monitor its formation and evolution (Aulicino and Wadhams, 2022). Regardless of the reasons for this new sea ice regime, the decline of SIE may have a range of impacts on the Ross Sea environment and biota. Ice shelves will undergo additional basal melting and instability due to greater exposure to waves, and changes in ocean stratification will alter circulation. Finally, the production of HSSW could change with direct implications on AABW and thermohaline circulation. Therefore, further work is needed to fill knowledge gaps and provide the basic information to improve future projections of sea ice changes and variability in the Ross Sea (Eayrs et al., 2021). Priorities include improved in situ observations over polynyas and pack ice from drifting buoys and autonomous underwater vehicles, higher resolution satellite imagery for coastal ice drift and deformation and more accurate sea ice and snow freeboard detection as a proxy for thickness (Farooq et al., 2020; Tian et al., 2020; Rack et al., 2021).

Future changes remain uncertain because the latest climate model projections do not account for dynamic ice sheet melting, and the properties and rate of formation of DSW and AABW are poorly represented by models (Purich and England, 2021). Winter observations are still lacking. Some fundamental processes that occur during winter (HSSW production, sea ice formation) are undersampled. Furthermore, a clear picture of the overall dynamics of the Ross Sea water masses is lacking, especially in terms of zonal connectivity. Freshwater enters through the eastern gate of the Ross Sea, but very little information is available on its characteristics and volume, and on its effect on the salinity budget, which ultimately determines the salinity of the DSW and consequently AABW formation.

## CRediT authorship contribution statement

**Pierpaolo Falco:** Writing – review & editing, Writing – original draft, Supervision, Investigation, Conceptualization. **Giuseppe Aulicino:** Writing – original draft, Methodology, Investigation, Formal analysis, Data curation, Conceptualization. **Pasquale Castagno:** Writing – original draft, Methodology, Investigation, Formal analysis, Data curation, Conceptualization. **Vincenzo Capozzi:** Writing – original draft, Supervision, Methodology, Formal analysis, Data curation, Conceptualization. **Paola de Ruggiero:** Writing – original draft, Methodology, Formal analysis, Data curation, Conceptualization. **Angela Garzia:** Writing – original draft, Methodology, Investigation, Formal analysis, Data curation, Conceptualization. **Antonino Ian Ferola:** Writing – original draft, Methodology, Formal analysis, Data curation, Conceptualization. **Yuri Cotroneo:** Writing – original draft, Methodology, Formal analysis, Data curation, Conceptualization. **Alessio Colella:** Writing – original draft, Methodology, Formal analysis, Data curation, Conceptualization. **Giannetta Fusco:** Writing – original draft, Supervision, Conceptualization. **Stefano Pierini:** Writing – original draft, Supervision, Investigation, Conceptualization. **Giorgio Budillon:** Writing – original draft, Supervision, Investigation, Conceptualization. **Enrico Zambianchi:** Writing – review & editing, Writing – original draft, Supervision, Investigation, Conceptualization. **Giancarlo Spezie:** Writing – original draft, Investigation, Conceptualization.

## Declaration of competing interest

The authors declare that they have no known competing financial interests or personal relationships that could have appeared to influence the work reported in this paper.

## Acknowledgements

We would like to thank the Italian Programme for Research in Antarctica (PNRA) for funding and supporting the logistics of numerous projects carried out in the Ross Sea from the early 1990s to the present, and all the researchers/technicians who contributed to the data collection. We would also like to thank Naomi Krauzig for her contribution to Table 1 and Fig. 1. We are grateful to the guest editor Walker O. Smith, Jr, for his help and constructive feedback.

## Data availability

No data was used for the research described in the article.

## References

Ackley, S.F., Stammerjohn, S., Maksym, T., Smith, M., Cassano, J., Guest, P., Tison, J.-L., Delille, B., Loose, B., Sedwick, P., DePace, L., Roach, L., Parno, J., 2021. Sea-ice production and air/ice/ocean/biogeochemistry interactions in the Ross Sea during the PIPERS 2017 autumn field campaign. Ann. Glaciol. 61 (82), 181–195. https://doi.org/10.1017/aog.2020.31.

Adusumilli, S., Fricker, H.A., Medley, B., Padman, L., Siegfried, M.R., 2020. Interannual variations in meltwater input to the Southern Ocean from Antarctic ice shelves. Nat. Geosci. 13 (9), 616–620.

Aoki, S., Yamazaki, K., Hirano, D., Katsumata, K., Shimada, K., Kitade, Y., Sasaki, H., Murase, H., 2020. Reversal of freshening trend of antarctic bottom water in the Australian-Antarctic Basin during 2010s. Sci. Rep. 10, 14415. https://doi.org/10.1038/s41598-020-71290-6.

Arblaster, J.M., Meehl, G.A., Karoly, D.J., 2011. Future climate change in the Southern Hemisphere: competing effects of ozone and greenhouse gases. Geophys. Res. Lett. 38, L02701. https://doi.org/10.1029/2010GL045384.

Arndt, J.E., Schenke, H.W., Jakobsson, M., Nitsche, F.O., Buys, G., Goleby, B., Rebesco, M., Bohoyo, F., Hong, J., Black, J., Greku, R., Udintsev, G., Barrios, F., Reynoso-Peralta, W., Taisei, M., Wigley, R., 2013. The International Bathymetric Chart of the Southern Ocean (IBCSO) Version 1.0 - a new bathymetric compilation covering circum-Antarctic water. Geophys. Res. Lett. 40, 3111–3117. https://doi.org/10.1002/grl.50413.

Arzeno, I.B., Beardsley, R.C., Limeburner, R., Owens, B., Padman, L., Springer, S.R., Stewart, C.L., Williams, M.J., 2014. Ocean variability contributing to basal melt rate near the ice front of Ross Ice Shelf, Antarctica. J. Geophys. Res.: Oceans 119, 4214–4233.

Assmann, K., Hellmer, H., Beckmann, A., 2003. Seasonal variation in circulation and water mass distribution on the Ross Sea continental shelf. Antarct. Sci. 15, 3–11.
Aulicino, G., Fusco, G., Kern, S., Budillon, G., 2014. Estimation of sea-ice thickness in Ross and Weddell seas from SSM/I brightness temperatures. IEEE Trans. Geosci. Rem. Sens. 52 (7), 4122–4140. https://doi.org/10.1109/TGRS.2013.2279799.
Aulicino, G., Sansiviero, M., Paul, S., Cesarano, C., Fusco, G., Wadhams, P., Budillon, G., 2018. A New approach for monitoring the Terra Nova Bay Polynya through MODIS ice surface temperature imagery and its validation during 2010 and 2011 winter seasons. Rem. Sens. 10, 366. https://doi.org/10.3390/rs10030366.
Aulicino, G., Wadhams, P., Parmiggiani, F., 2019. SAR pancake ice thickness retrieval in the terra nova bay (Antarctica) during the PIPERS expedition in winter 2017. Rem. Sens. 11 (21), 2510. https://doi.org/10.3390/rs11212510.
Aulicino, G., Wadhams, P., 2022. Editorial for the special issue "remote sensing of the polar oceans". Rem. Sens. 14, 6195. https://doi.org/10.3390/rs14246195.
Ayres, H.C., Screen, J.A., Blockley, E.W., Bracegirdle, T.J., 2022. The coupled atmosphere–ocean response to antarctic sea ice loss. J. Clim. 35, 4665–4685. https://doi.org/10.1175/JCLI-D-21-0918.1.
Baldacchino, F., Morlighem, M., Golledge, N.R., Horgan, H., Malyarenko, A., 2022. Sensitivity of the Ross ice shelf to environmental and glaciological controls. Cryosphere 16, 3723–3738. https://doi.org/10.5194/tc-16-3723-2022.
Bergamasco, A., Defendi, V., Meloni, R., 2002. Some dynamics of water outflow from beneath the Ross ice shelf during 1995 and 1996. Antarct. Sci. 14, 74–82. https://doi.org/10.1017/S0954102002000603.
Bertler, N.A.N., Barrett, P.J., Mayewski, P.A., Fogt, R.L., Kreutz, K.J., Shulmeister, J., 2004. El niño suppresses antarctic warming. Geophys. Res. Lett. 31, L15207. https://doi.org/10.1029/2004GL020749.
Bowen, M.M., Fernandez, D., Vazquez, A.F., Gordon, A.L., Huber, B., Castagno, P., Falco, P., 2021. The role of tides in bottom water export from the western Ross Sea. Sci. Rep. 11, 2246. https://doi.org/10.1038/s41598-021-81793-5.
Bowen, M.M., Fernandez, D., Gordon, A.L., Huber, B., Castagno, P., Falco, P., Budillon, G., Gunn, K.L., Forcen-Vazquez, A., 2023. Tides regulate the flow and density of antarctic bottom water from the western Ross Sea. Sci. Rep. 13, 3873. https://doi.org/10.1038/s41598-023-31008-w.
Brett, G.M., Irvin, A., Rack, W., Haas, C., Langhorne, P.J., Leonard, G.H., 2020. Variability in the distribution of fast ice and the sub-ice platelet layer near McMurdo ice shelf. J. Geophys. Res.: Oceans 125, e2019JC015678. https://doi.org/10.1029/2019JC015678.
Budillon, G., Spezie, G., 2000. Thermohaline structure and variability in the terra nova bay polynya, Ross Sea. Antarct. Sci. 12 (4), 493–508. https://doi.org/10.1017/S0954102000000572.
Budillon, G., Fusco, G., Spezie, G., 2000. A study of surface heat fluxes in the Ross Sea (Antarctica). Antarct. Sci. 12 (2), 243–254.
Budillon, G., Gremes Cordero, S., Salusti, E., 2002. On the dense water spreading off the Ross Sea shelf (Southern Ocean). J. Mar. Syst. 35, 207–227. https://doi.org/10.1016/S0924-7963(02)00082-9.
Budillon, G., Pacciaroni, M., Cozzi, S., Rivaro, P., Catalano, G., Ianni, C., Cantoni, C., 2003. An optimum multiparameter mixing analysis of the shelf waters in the Ross Sea. Antarct. Sci. 15, 105–118. https://doi.org/10.1017/S095410200300110X.
Budillon, G., Salusti, E., Tucci, S., 2006. The evolution of density currents and nepheloid bottom layers in the Ross Sea (Antarctica). J. Mar. Res. 64 (4), 517–540.
Budillon, G., Castagno, P., Aliani, S., Spezie, G., Padman, L., 2011. Thermohaline variability and Antarctic bottom water formation at the Ross Sea shelf break. Deep. Res. I 58, 1002–1018. https://doi.org/10.1016/j.dsr.2011.07.002.
Burada, G.K., McDonald, A., Renwick, J., Jolly, B., 2023. Delineating polynya area using active and passive microwave sensors for the western Ross Sea sector of Antarctica. Rem. Sens. 15, 2545. https://doi.org/10.3390/rs15102545.
Cai, W., Van Rensch, P., Cowan, T., Hendon, H.H., 2011. Teleconnection pathways of ENSO and the IOD and the mechanisms for impacts on Australian rainfall. J. Clim. 24, 3910–3923. https://doi.org/10.1175/2011JCLI4129.1.
Capello, M., Budillon, G., Cutroneo, L., Tucci, S., 2009. The nepheloid bottom layer and water masses at the shelf break of the western Ross Sea. Deep-Sea Res. 56, 843–858. https://doi.org/10.1016/j.dsr2.2008.10.032.
Carret, A., Llovel, W., Penduff, T., Molines, J.-M., 2021. Atmospherically forced and chaotic interannual variability of regional sea level and its components over 1993–2015. J. Geophys. Res.: Oceans 126, e2020JC017123.
Castagno, P., Capozzi, V., Ditullio, G.R., Falco, P., Fusco, G., Rintoul, S.R., Spezie, G., Budillon, G., 2019. Rebound of shelf water salinity in the Ross Sea. Nat. Commun. 1, 6. https://doi.org/10.1038/s41467-019-13083-8.
Castagno, P., Falco, P., Dinniman, M.S., Spezie, G., Budillon, G., 2017. Temporal variability of the circumpolar deep water inflow onto the Ross Sea continental shelf. J. Mar. Syst. 166, 37–49. https://doi.org/10.1016/j.jmarsys.2016.05.006.
Castellani, G., Losch, M., Ungermann, M., Gerdes, R., 2018. Sea-ice drag as a function of deformation and ice cover: effects on simulated sea ice and ocean circulation in the Arctic. Ocean Model. 128, 48–66. https://doi.org/10.1016/j.ocemod.2018.06.002.
Cerrone, D., Fusco, G., Simmonds, I., Aulicino, G., Budillon, G., 2017. Dominant covarying climate signals in the southern Ocean and antarctic Sea Ice influence during the last three decades. J. Clim. 30, 3055–3072. https://doi.org/10.1175/JCLI-D-16-0439.1.
Cerrone, D., Fusco, G., 2018. Low-frequency climate modes and antarctic Sea Ice variations, 1982–2013. J. Clim. 31, 147–175. https://doi.org/10.1175/JCLI-D-17-0184.1.
Ciappa, A., Budillon, G., 2012. The Terra Nova Bay (Antarctica) Polynya observed by MODIS ice surface temperature imagery from may to June 2009. Int. J. Rem. Sens. 33 (14), 4567–4582. https://doi.org/10.1080/01431161.2011.652314.
Ciappa, A., Pietranera, L., Budillon, G., 2012. Observations of the terra nova bay (Antarctica) polynya by MODIS ice surface temperature imagery from 2005 to 2010. Remote Sens. Environ. 119, 158–172. https://doi.org/10.1016/j.rse.2011.12.017.
Clem, K.R., Fogt, R.L., 2015. South Pacific circulation changes and their connection to the tropics and regional Antarctic warming in austral spring, 1979-2012. J. Geophys. Res. 120, 2773–2792. https://doi.org/10.1002/2014JD022940.
Clem, K.R., Renwick, J.A., McGregor, J., Fogt, R.L., 2016. The relative influence of ENSO and SAM on Antarctic Peninsula climate. J. Geophys. Res. Atmos. 121, 9324–9341. https://doi.org/10.1002/2016JD025305.
Clough, J.W., Hansen, B.L., 1979. The Ross ice shelf project. Science 203, 433–434.
Cohen, L., Dean, S., Renwick, J., 2013. Synoptic weather types for the Ross Sea region, Antarctica. J. Clim. 26, 636–649. https://doi.org/10.1175/JCLI-D-11-00690.1.
Commodari, V., Pierini, S., 1999. A wind and boundary driven circulation model of the Ross Sea. In: Spezie, G., Manzella, G.M.R. (Eds.), Oceanography of the Ross Sea (Antarctica). Springer-Verlag, pp. 135–144, 88-470-0039-4.
Cullather, R.I., Bromwich, D.H., Van Woert, M.L., 1996. Interannual variations in antarctic precipitation related to El niño-southern oscillation. J. Geophys. Res. Atmos. 101 (D14), 19109–19118.
Danabasoglu, G., et al., 2020. The community Earth system model version 2 (CESM2). J. Adv. Model. Earth Syst. 12 (2), e2019MS001. https://doi.org/10.1029/2019MS001916.
Das, I., Padman, L., Bell, R.E., Fricker, H.A., Tinto, K.J., Hulbe, C.L., Siddoway, C.S., Dhakal, T., Frearson, N.P., Mosbeux, C., Cordero, S.I., Siegfried, M.S., 2020. Multidecadal basal melt rates and structure of the Ross Ice Shelf, Antarctica, using airborne ice penetrating radar. J. Geophys. Res.: Earth 125, e2019JF005241. https://doi.org/10.1029/2019JF005241.
Ding, Q., Steig, E.J., 2013. Temperature change on the antarctic Peninsula linked to the tropical pacific. J. Clim. 26, 7570–7585. https://doi.org/10.1175/JCLI-D-12-00729.1.
Dinniman, M.S., Klinck, J.M., Smith Jr., W.O., 2003. Cross-shelf exchange in a model of the Ross Sea circulation and biogeochemistry. Deep-Sea Res. 50, 3103–3120.
Dinniman, M.S., Klinck, J.M., Smith Jr., W.O., 2007. Influence of sea ice cover and icebergs on circulation and water mass formation in a numerical circulation model of the Ross Sea, Antarctica. J. Geophys. Res.:Oceans 112, C11.
Dinniman, M.S., Klinck, J.M., Smith Jr., W.O., 2011. A model study of circumpolar deep water on the West antarctic Peninsula and Ross Sea continental shelves. Deep-Sea Res. 58, 1508–1523.
Dinniman, M.S., Klinck, J.M., Hofmann, E.E., Smith Jr., W.O., 2018. Effects of projected changes in wind, atmospheric temperature, and freshwater inflow on the Ross Sea. J. Clim. 31 (4), 1619–1635. https://doi.org/10.1175/JCLI-D-17-0351.1.
Dotto, T.S., Naveira Garabato, A., Bacon, S., Tsamados, M., Holland, P.R., Hooley, J., Frajka-Williams, E., Tsamados, M., Ridout, A., Meredith, M., 2018. Variability of the Ross gyre, Southern Ocean: drivers and responses revealed by satellite altimetry. Geophys. Res. Lett. 45, 6195–6204.
DuVivier, A.K., Molina, M.J., Deppenmeier, A.L., Holland, M., Landrum, L., Krumhardt, K., Jenouvrier, S., 2024. Projections of winter polynyas and their biophysical impacts in the Ross Sea Antarctica. Clim. Dynam. 62, 989–1012. https://doi.org/10.1007/s00382-023-06951-z.
Eayrs, C., Li, X., Raphael, M.N., Holland, D.M., 2021. Rapid decline in Antarctic sea ice in recent years hints at future change. Nat. Geosci. 14, 460–464. https://doi.org/10.1038/s41561-021-00768-3.
Falco, P., Krauzig, N., Castagno, P., Garzia, A., Martellucci, R., Cotroneo, Y., Flocco, D., Menna, M., Pirro, A., Mauri, E., Memmola, F., Solidoro, C., Pacciaroni, M., Notarstefano, G., Budillon, G., Zambianchi, E., 2024. Filling the Gap: Winter Thermohaline Evolution along and below the Ross Ice Shelf. Nat. Commun. in press.
Farooq, U., Rack, W., McDonald, A., Howell, S., 2020. Long-term analysis of Sea Ice drift in the western Ross Sea, Antarctica, at high and low spatial resolution. Rem. Sens. 12, 1402. https://doi.org/10.3390/rs12091402.
Farooq, U., Rack, W., McDonald, A., Howell, S., 2023. Representation of sea ice regimes in the Western Ross Sea, Antarctica, based on satellite imagery and AMPS wind data. Clim. Dynam. 60, 227–238. https://doi.org/10.1007/s00382-022-06319-9.
Ferola, A.I., Cotroneo, Y., Wadhams, P., Fusco, G., Falco, P., Budillon, G., Aulicino, G., 2023. The role of the pacific-antarctic ridge in establishing the northward extent of Antarctic sea-ice. Geophys. Res. Lett. 50 (10), e2023GL104373. https://doi.org/10.1029/2023GL104373.
Ferrari, R., Jansen, M.F., Thompson, A.F., 2014. Antarctic sea ice control on ocean circulation in present and glacial climates. Proc. Natl. Acad. Sci. USA 111, 8753–8758.
Fogt, R.L., Wovrosh, A.J., Langen, R.A., Simmonds, I., 2012. The characteristic variability and connection to the underlying synoptic activity of the Amundsen-Bellingshausen Seas low. J. Geophys. Res. 117, D07111. https://doi.org/10.1029/2011JD017337.
Fonseca, R., Francis, D., Aulicino, G., Mattingly, K.S., Fusco, G., Budillon, G., 2023. Atmospheric controls on the terra nova bay polynya occurrence in Antarctica. Clim. Dynam. 61, 5147–5169. https://doi.org/10.1007/s00382-023-06845-0.
Fusco, G., Flocco, D., Budillon, G., Spezie, G., Zambianchi, E., 2002. Dynamics and variability of terra nova bay polynya. Mar. Ecology 23, 201–209. https://doi.org/10.1111/j.1439-0485.2002.tb00019.x.
Fusco, G., Budillon, G., Spezie, G., 2009. Surface heat fluxes and thermohaline variability in the Ross Sea and in terra nova bay polynya. Continent. Shelf Res. 29 (15), 1887–1895. https://doi.org/10.1016/j.csr.2009.07.006.
Gordon, A.L., Comiso, J.C., 1988. Polynyas in the Southern Ocean. Sci. Am. 258 (6), 90–97. https://doi.org/10.1038/scientificamerican0688-90.
Gordon, A.L., Orsi, A.H., Muench, R., Huber, B., Zambianchi, E., Visbeck, M., 2009. Western Ross Sea continental slope gravity currents. Deep Sea Res. 56, 796–817. https://doi.org/10.1016/j.dsr2.2008.10.037.

Gordon, A.L., Huber, B., Busecke, J., 2015. Bottom water export from the western Ross Sea, 2007 through 2010. Geophys. Res. Lett. 42, 5387–5394. https://doi.org/10.1002/2015GL064457.
Greene, C.A., Gwyther, D.E., Blankenship, D.D., 2017. Antarctic mapping tools for matlab. Comput. Geosci. 104, 151–157. https://doi.org/10.1016/j.cageo.2016.08.003.
Griggs, J., Bamber, J., 2011. Antarctic ice-shelf thickness from satellite radar altimetry. J. Glaciol. 57, 485–498.
Guest, P., 2021. Inside katabatic winds over the Terra Nova Bay Polynya: 1. Atmospheric jet and surface conditions. J. Geophys. Res. Atmos. 126, e2021JD034902. https://doi.org/10.1029/2021JD034902ù.
Gunn, K.L., Rintoul, S.R., England, M.H., Bowen, M.M., 2023. Recent reduced abyssal overturning and ventilation in the Australian Antarctic Basin. Nat. Clim. Change 13, 537–544. https://doi.org/10.1038/s41558-023-01667-8.
Guo, G., Gao, L., Shi, J., 2020. Modulation of dense shelf water salinity variability in the western Ross Sea associated with the Amundsen Sea Low. Environ. Res. Lett. 16 (1), 014004.
Heil, P., Stevens, C., Lee, W.S., Eayrs, C., Shin, H.C., Alexander, S.P., Rack, W., 2023. Bridging the gap for ice–ocean–ecosystem processes: integrated observing system for the Ross Sea-far East Antarctic Region. Front. Mar. Sci. 10, 1206119. https://doi.org/10.3389/fmars.2023.1206119.
Henley, B.J., Gergis, J., Karoly, D.J., Power, S., Kennedy, J., Folland, C.K., 2015. A tripole index for the interdecadal pacific oscillation. Clim. Dynam. 45, 3077–3090. https://doi.org/10.1007/s00382-015-2525-1.
Heuzé, C., Heywood, K.J., Stevens, D.P., Ridley, J.K., 2013. Southern Ocean bottom water characteristics in CMIP5 models. Geophys. Res. Lett. 40, 1409–1414.
Himmich, K., Vancoppenolle, M., Madec, G., Sallée, J.B., Holland, P.R., Lebrun, M., 2023. Drivers of Antarctic sea ice advance. Nat. Commun. 14, 6219. https://doi.org/10.1038/s41467-023-41962-8.
Holland, D.M., Jacobs, S.S., Jenkins, A., 2003. Modelling the ocean circulation beneath the Ross ice shelf. Antarct. Sci. 15, 13–23.
Hobbs, W., Massom, R., Stammerjohn, S., Reid, P., Williams, G.D., Meier, W.N., 2016. A review of recent changes in Southern Ocean Sea Ice, their drivers and forcings. Global Planet. Change 143, 228–250. https://doi.org/10.1016/j.gloplacha.2016.06.008.
Hobbs, W., Spence, P., Meyer, A., Schroeter, S., Fraser, A.D., Reid, P., Tian, T.R., Wang, Z., Liniger, G., Doddridge, E.W., Boyd, P.W., 2024. Observational evidence for a regime shift in summer antarctic Sea Ice. J. Clim. 37, 2263–2275. https://doi.org/10.1175/JCLI-D-23-0479.1.
Hogg, A. McC., Penduff, T., Close, S.E., Dewar, W.K., Constantinou, N.C., Martínez-Moreno, J., 2022. Circumpolar variations in the chaotic nature of Southern Ocean eddy dynamics. J. Geophys. Res.: Oceans 127, e2022JC018440.
Inserra, G., Buono, A., Nunziata, F., Migliaccio, M., Parmiggiani, F., Aulicino, G., 2024. Characterization of the Terra Nova Bay polynya using dual-polarimetric C-band SAR measurements. IEEE J. Ocean. Eng. 49 (3), 856–869. https://doi.org/10.1109/JOE.2024.3356569.
Irving, D., Simmonds, I., 2016. A new method for identifying the pacific–south American pattern and its influence on regional climate variability. J. Clim. 29, 6109–6125. https://doi.org/10.1175/JCLI-D-15-0843.1.
Jacobs, S.S., Amost, A.F., Bruchhausen, P.M., 1970. Ross Sea oceangoraphy and antarctic bottom water formation. Deep Sea Res. 17, 935–962.
Jacobs, S.S., Gordon, A.L., Ardai, J., 1979. Circulation and melting beneath the Ross ice shelf. Science 203, 439–443. https://doi.org/10.1126/science.203.4379.439.
Jacobs, S.S., Fairbanks, G., 1985. Origin and evolution of water masses near the Antarctic continental margin: evidence from H218O/H216O ratios in seawater. Oceanol. Antarct. Cont. Shelf 43, 59–85.
Jacobs, S.S., Comiso, J.C., 1989. Sea ice and oceanic processes on the Ross Sea continental shelf. J. Geophys. Res. 94, 18195–18211. https://doi.org/10.1029/jc094ic12p18195.
Jacobs, S.S., Hellmer, H.H., Doake, C.S.M., Jenkins, A., Frolich, R.M., 1992. Melting of ice shelves and the mass balance of Antarctica. J. Glaciol. 38, 375–387.
Jacobs, S.S., Giulivi, C.F., 2010. Large multidecadal salinity trends near the Pacific-Antarctic continental margin. J. Clim. 23 (17), 4508–4524. https://doi.org/10.1175/2010JCLI3284.1.
Jacobs, S.S., Giulivi, C.F., Dutrieux, P., 2022. Persistent Ross Sea freshening from imbalance West Antarctic ice shelf melting. J. Geophys. Res. 126, 3. https://doi.org/10.1029/2021JC017808.
Jendersie, S., Williams, M., Langhorne, P.J., Robertson, R., 2018. The density-driven winter intensification of the Ross Sea circulation. J. Geophys. Res.: Oceans 123, 7702–7724.
Jenkins, A., Dutrieux, P., Jacobs, S.S., McPhail, S.D., Perrett, J.R., Webb, A.T., White, D., 2010. Observations beneath pine Island Glacier in west Antarctica and implications for its retreat. Nat. Geosci. 3, 468–472.
Jin, D., Kirtman, B.P., 2009. Why the southern Hemisphere ENSO responses lead ENSO. J. Geophys. Res. 114, D23101. https://doi.org/10.1029/2009JD012657.
Johnson, G.C., 2008. Quantifying antarctic bottom water and north atlantic deep water volumes. J. Geophys. Res. 113, C05027.
Joughin, I., Smith, B.E., Medley, B., 2014. Marine ice sheet collapse potentially under way for the Thwaites Glacier basin, West Antarctica. Science 344, 735–738. https://doi.org/10.1126/science.1249055.
Kaleschke, L., Tian-Kunze, X., Maaß, N., Mäkynen, M., Drusch, M., 2012. Sea ice thickness retrieval from SMOS brightness temperatures during the Arctic freeze-up period. Geophys. Res. Lett. 39, L05501. https://doi.org/10.1029/2012GL050916.
Kern, S., Aliani, S., 2011. A comparison between polynya area and associated ice production with mooring-based measurements of temperature, salinity and currents in the southwestern Ross Sea, Antarctica. Ann. Glaciol. 52 (57), 291–300. https://doi.org/10.3189/172756411795931705.
Kern, S., Ozsoy-Çiçek, B., 2016. Satellite remote sensing of snow depth on antarctic Sea Ice: an inter-comparison of two empirical approaches. Rem. Sens. 8, 450. https://doi.org/10.3390/rs8060450.
Klinck, J.M., Dinniman, M.S., 2010. Exchange across the shelf break at high southern latitudes. Ocean Sci. 6, 513–524. https://doi.org/10.5194/os-6-513-2010.
Knuth, S.L., Cassano, J.J., 2014. Estimating sensible and latent heat fluxes using the integral method from in situ aircraft measurements. J. Atmos. Ocean. Technol. 31 (9), 1964–1981. https://doi.org/10.1175/jtech-d-14-00008.1.
Kohut, J., Hunter, E., Huber, B., 2013. Small-scale variability of the cross-shelf flow over the outer shelf of the Ross Sea. J. Geophys. Res.: Oceans 118, 1863–1876. https://doi.org/10.1002/jgrc.20090.
Kurtz, D.D., Bromwich, D.H., 1983. Satellite observed behavior of the terra nova bay polynya. J. Geophys. Res. 88, 9717–9722.
Kurtz, N.T., Markus, T., 2012. Satellite observations of Antarctic sea ice thickness and volume. J. Geophys. Res. 117, C08025. https://doi.org/10.1029/2012JC008141.
Langhorne, P.J., Haas, C., Price, D., Rack, W., Leonard, G.H., Brett, G.M., Urbini, S., 2023. Fast ice thickness distribution in the western Ross Sea in late spring. J. Geophys. Res.: Oceans 128, e2022JC019459. https://doi.org/10.1029/2022JC019459.
Lecomte, O., Goosse, H., Fichefet, T., de Lavergne, C., Barthélemy, A., Zunz, V., 2017. Vertical ocean heat redistribution sustaining sea-ice concentration trends in the Ross Sea. Nat. Commun. 8, 258. https://doi.org/10.1038/s41467-017-00347-4.
Lee, H.-J., Jin, E.K., 2023. Understanding the delayed Amundsen Sea low response to ENSO. Front. Earth Sci. 11. https://doi.org/10.3389/feart.2023.1136025.
Leonard, G.H., Turner, K.E., Richter, M.E., Whittaker, M.S., Smith, I.J., 2021. Brief communication: the anomalous winter 2019 seaice conditions in McMurdo Sound, Antarctica. Cryosphere 15 (10), 4999–5006. https://doi.org/10.5194/tc-15-4999-2021.
Li, X., Holland, D.M., Gerber, E.P., Yoo, C., 2014. Impacts of the north and tropical atlantic ocean on the antarctic Peninsula and sea ice. Nature 505, 538–542. https://doi.org/10.1038/nature12945.
Li, X., Gerber, E.P., Holland, D.M., Yoo, C., 2015. A Rossby wave bridge from the tropical Atlantic to West Antarctica. J. Clim. 28, 2256–2273. https://doi.org/10.1175/JCLI-D-14-00450.1.
Li, X., et al., 2021. Tropical teleconnection impacts on Antarctic climate changes. Nat. Rev. Earth Environ. 2, 680–698. https://doi.org/10.1038/s43017-021-00204-5.
Li, Y., McGillicuddy, D.J., Dinniman, M.S., Klinck, J.M., 2017. Processes influencing formation of low-salinity high-biomass lenses near the edge of the Ross Ice Shelf. J. Mar. Syst. 166, 108–119. https://doi.org/10.1016/j.jmarsys.2016.07.002.
Li, Z., England, M.H., Hog, A.M., Rintoul, S.R., Morrison, A.K., 2023. Abyssal ocean overturning slowdown and warming driven by Antarctic meltwater. Nature 615. https://doi.org/10.1038/s41586-023-05762-w.
Lin, Y., Yang, Q., Mazloff, M., Wu, X., Tian-Kunze, X., Kaleschke, L., Yu, L., Chen, D., 2023. Transiting consolidated ice strongly influenced polynya area during a shrink event in Terra Nova Bay in 2013. Commun. Earth Environ. 4, 54. https://doi.org/10.1038/s43247-023-00712-w.
Liu, J., Zhu, Z., Chen, D., 2023. Lowest antarctic Sea Ice record broken for the second year in a row. Ocean-Land-Atmos. Res. 2, 7. https://doi.org/10.34133/olar.0007.
Locarnini, R.A., 1994. Water masses and circulation in the Ross gyre and environs. MS thesis. Texas A and M University, College Station, p. 87.
Lumpkin, R., Speer, K., 2007. Global ocean meridional overturning. J. Phys. Oceanogr. 37, 2550–2562. https://doi.org/10.1175/JPO3130.1.
Malyarenko, A., Robinson, N.J., Williams, M.J.M., Langhorne, P.J., 2019. A wedge mechanism for summer surface water inflow into the Ross Ice Shelf cavity. J. Geophys. Res. 124, 1196–1214.
Malyarenko, A., Gossart, A., Sun, R., Krapp, M., 2023. Conservation of heat and mass in P-SKRIPS. version 1: the coupled atmosphere–ice–ocean model of the Ross Sea. Geosci. Model Dev. (GMD) 16, 3355–3373. https://doi.org/10.5194/gmd-16-3355-2023.
Martin, S., 2019. Polynyas. In: Cochran, J.K., Bokuniewicz, H.J., Yager, P.L. (Eds.), Encyclopedia of Ocean Sciences, third ed. Academic Press, Oxford, pp. 175–180. https://doi.org/10.1016/B978-0-12-409548-9.11477-0.
Marshall, J., Adcroft, A., Hill, C., Perelman, L., Heisey, C., 1997. A finite-volume, incompressible Navier Stokes model for studies of the ocean on parallel computers. J. Geophys. Res. Oceans 102, 5753–5766.
Marshall, J., Speer, K., 2012. Closure of the meridional overturning circulation through Southern Ocean upwelling. Nat. Geosci. 5, 171–180.
Marshall, G.J., Thompson, D.W.J., 2016. The signatures of large-scale patterns of atmospheric variability in Antarctic surface temperatures. J. Geophys. Res. Atmos. 121, 3276–3289. https://doi.org/10.1002/2015JD024665.
Massom, R., Stammerjohn, S., Lefebvre, W., Harangozo, S.A., Adams, N., Scambos, T.A., Pook, M.J., Fowler, C., 2008. West Antarctic Peninsula sea ice in 2005: extreme ice compaction and ice edge retreat due to strong anomaly with respect to climate. J. Geophys. Res. 113, C02S20. https://doi.org/10.1029/2007JC004239.
Massom, R., Stammerjohn, S., 2010. Antarctic sea ice change and variability – physical and ecological implications. Pol. Sci. 4 (2), 149–186. https://doi.org/10.1016/j.polar.2010.05.001.
McFarquhar, G.M., et al., 2021. Observations of clouds, aerosols, precipitation, and surface radiation over the southern ocean: an overview of capricorn, marcus, micre, and socrates. Bull. Am. Meteorol. Soc. 102, E894–E928. https://doi.org/10.1175/BAMS-D-20-0132.1.
McGillicuddy Jr., D.J., Budillon, G., Kustka, A., 2017. Mesoscale and high-frequency variability in the Ross Sea (Antarctica): an introduction to the special issue. J. Mar. Syst. 166, 1–3.

Meccia, V.L., Fuentes-Franco, R., Davini, P., Bellomo, K., Fabiano, F., Yang, S., von Hardenberg, J., 2023. Internal multi-centennial variability of the atlantic meridional overturning circulation simulated by EC-earth3. Clim. Dynam. 60, 3695–3712. https://doi.org/10.1007/s00382-022-06534-4.

Meehl, G.A., Arblaster, J.M., Bitz, C.M., Chung, C.T., Teng, H., 2016. Antarctic sea-ice expansion between 2000 and 2014 driven by tropical Pacific decadal climate variability. Nat. Geosci. 9, 590–595. https://doi.org/10.1038/ngeo2751.

Miller, U.K., Zappa, C.J., Gordon, A.L., Yoon, S.T., Stevens, C., Lee, W.S., 2024. High salinity shelf water production rates in terra nova bay, Ross Sea from high-resolution salinity observations. Nat. Commun. 15 (1), 373.

Mo, K.C., 2000. Relationships between low-frequency variability in the southern Hemisphere and sea surface temperature anomalies. J. Clim. 13, 3599–3610. https://doi.org/10.1175/1520-0442(2000)013<3599:RBLFVI>2.0.CO;2.

Morales Maqueda, M.A., Willmott, A.J., Biggs, N.R.T., 2004. Polynya dynamics: a review of observations and modeling. Rev. Geophys. 42, RG1004. https://doi.org/10.1029/2002RG000116.

Muench, R., Padman, L., Gordon, A.L., Orsi, A.H., 2009. A dense water outflow from the Ross Sea, Antarctica: mixing and the contribution of tides. J. Mar. Syst. 77, 369–387. https://doi.org/10.1016/j.jmarsys.2008.11.003.

Nelson, M.J.S., Queste, B.Y., Smith, I.J., Leonard, G.H., Webber, B.G.M., Hughes, K.G., 2017. Measurements of ice shelf water beneath the front of the Ross ice shelf using gliders. Ann. Glaciol. 58 (74), 41–50. https://doi.org/10.1017/aog.2017.34.

Newson, K.L., Francavillese, L., Tiernei, J., 1965. Operation Deep Freeze 62. 1961-62 Marine Geophysical Investigation, R-118. US Naval Oceanogr. Off, p. 157 (unpublished Manuscript.

Nihashi, S., Ohshima, K.I., Tamura, T., 2024. Reconstruct the AMSR-E/2 thin ice thickness algorithm to create a long-term time series of sea-ice production in Antarctic coastal polynyas. Pol. Sci. 39, 100978. https://doi.org/10.1016/j.polar.2023.100978.

Nuncio, M., Yuan, X., 2015. The influence of the Indian Ocean dipole on Antarctic sea ice. J. Clim. 28, 2682–2690. https://doi.org/10.1175/JCLI-D-14-00390.1.

Ohshima, K.I., Nihashi, S., Iwamoto, K., 2016. Global view of sea-ice production in polynyas and its linkage to dense/bottom water formation. Geosci. Lett. 3, 13. https://doi.org/10.1186/s40562-016-0045-4.

Orsi, A.H., Johnson, G.C., Bullister, J.L., 1999. Circulation, mixing, and production of Antarctic bottom water. Prog. Oceanogr. 43, 55–109.

Orsi, A.H., Smethie, Jr W.M., Bullister, J.L., 2002. On the total input of Antarctic waters to the deep ocean: a preliminary estimate from chlorofluorocarbon measurements. J. Geophys. Res. 107, C8. https://doi.org/10.1029/2001JC000976.

Orsi, A.H., Whitworth, T., Nowlin, W.D., 1995. On the meridional extent and fronts of the Antarctic. Circumpolar Current. Deep-Sea Res. I 42 (5), 641–673. https://doi.org/10.1016/0967-0637(95)00021-W.

Orsi, A.H., Wiederwohl, C.L., 2009. A recount of Ross Sea waters. Deep Sea Res. 56, 778–795. https://doi.org/10.1016/j.dsr2.2008.10.033.

Padman, L., Howard, S.L., Orsi, A.H., Muench, R., 2009. Tides of the northwestern Ross Sea and their impact on dense outflows of antarctic bottom water. Deep Sea Res. 56, 818–834. https://doi.org/10.1016/j.dsr2.2008.10.026.

Paolo, F.S., Fricker, H.A., Padman, L., 2015. Volume loss from Antarctic ice shelves is accelerating. Science 348 (6232), 327–331. https://doi.org/10.1126/science.aaa0940.

Park, J., Kim, H.C., Jo, Y.H., Kidwell, A., Hwang, J., 2018. Multi-temporal variation of the Ross Sea Polynya in response to climate forcings. Polar Res. 37 (1), 1444891.

Park, J.Y., Schloesser, F., Timmermann, A., Choudhury, D., Lee, J.Y., Nellikkattil, A.B., 2023. Future sea-level projections with a coupled atmosphere-ocean-ice-sheet model. Nat. Commun. 14, 636. https://doi.org/10.1038/s41467-023-36051-9.

Parkinson, C.L., Cavalieri, D.J., 2012. Antarctic Sea ice variability and trends, 1979–2010. Cryosphere 6 (4), 871–880. https://doi.org/10.5194/tc-6-871-2012.

Parkinson, C.L., 2019. A 40-y record reveals gradual Antarctic sea ice increases followed by decreases at rates far exceeding the rates seen in the Arctic. Proc. Natl. Acad. Sci. USA 116 (29), 14.414–14.423. https://doi.org/10.1073/pnas.1906556116.

Paul, S., Hendricks, S., Ricker, R., Kern, S., Rinne, E., 2018. Empirical parametrization of envisat freeboard retrieval of Arctic and Antarctic sea ice based on CryoSat-2: progress in the ESA climate change initiative. Cryosphere 12 (7), 2437–2460. https://doi.org/10.5194/tc-12-2437-2018.

Pillsbury, R.D., Jacobs, S.S., 1985. Preliminary observations from long-term current meter moorings near the Ross ice shelf, Antarctica. In: Jacobs, S.S. (Ed.), Oceanology of the Antarctic Continental Shelf. American Geophysical Union, pp. 87–107. https://doi.org/10.1029/AR043p0087.

Prend, C.J., et al., 2024. Ross Gyre variability modulates oceanic heat supply toward the West Antarctic continental shelf. Commun. Earth Environ. 5, 47.

Purich, A., England, M.H., Cai, W., Chikamoto, W., Timmermann, A., Fyfe, J.C., Frankcombe, L., Meehl, G.A., Arblaster, J.M., 2016. Tropical pacific SST drivers of recent antarctic Sea Ice trends. J. Clim. 29, 8931–8948. https://doi.org/10.1175/JCLI-D-16-0440.1.

Purich, A., England, M.H., 2021. Historical and future projected warming of antarctic shelf bottom water in CMIP6 models. Geophys. Res. Lett. 48, 10. https://doi.org/10.1029/2021GL092752.

Purich, A., Doddridge, E.W., 2023. Record low Antarctic Sea ice coverage indicates a new sea ice state. Commun. Earth Environ. 4, 314. https://doi.org/10.1038/s43247-023-00961-9.

Purkey, S.G., Johnson, G.C., 2012. Global contraction of Antarctic bottom water between the 1980s and 2000s. J. Clim. 25, 5830–5844.

Purkey, S.G., Johnson, G.C., 2013. Antarctic bottom water warming and freshening: contributions to sea level rise, ocean freshwater budgets, and global heat gain. J. Clim. 26, 6105–6122.

Qi, M., Liu, Y., Liu, J., Cheng, X., Lin, Y., Feng, Q., Shen, Q., Yu, Z., 2021. A 15-year circum-Antarctic iceberg calving dataset derived from continuous satellite observations. Earth Syst. Sci. Data 13, 4583–4601. https://doi.org/10.5194/essd-13-4583-2021.

Rack, W., Price, D., Haas, C., Langhorne, P.J., Leonard, G.H., 2021. Sea ice thickness in the western Ross Sea. Geophys. Res. Lett. 48, e2020GL090866. https://doi.org/10.1029/2020GL090866.

Raphael, M.N., Hobbs, W., 2014. The influence of the large-scale atmospheric circulation on Antarctic sea ice during ice advance and retreat seasons. Geophys. Res. Lett. 41 (14), 5037–5045.

Raphael, M.N., Handcock, M.S., 2022. A new record minimum for Antarctic sea ice. Nat. Rev. Earth Environ. 3, 215–216. https://doi.org/10.1038/s43017-022-00281-0.

Reese, R., Albrecht, T., Mengel, M., Asay-Davis, X., Winkelmann, R., 2018. Antarctic sub-shelf melt rates via PICO. Cryosphere 12 (6), 1969–1985. https://doi.org/10.5194/tc-12-1969-2018.

Rignot, E., Jacobs, S., Mouginot, J., Scheuchl, B., 2013. Ice-shelf melting around Antarctica. Science 341 (6143), 266–270. https://doi.org/10.1126/science.1235798.

Rignot, E., Mouginot, J., Scheuchl, B., Van Den Broeke, M., Van Wessem, M.J., Morlighem, M., 2019. Four decades of antarctic ice sheet mass balance from 1979–2017. P. Natl. Acad. Sci. 116 (4), 1095–1103.

Rivaro, P., Bergamasco, A., Budillon, G., Frache, R., Hohmann, R., Massolo, S., Spezie, G., 2004. Chlofofluorocarbon distribution in the Ross Sea water masses. Chem. Ecol. 20 (Suppl. 1), 1–13.

Rivaro, P., Massolo, S., Bergamasco, A., Castagno, P., Budillon, G., 2010. Chemical evidence of the changes of the antarctic bottom water ventilation in the western Ross Sea between 1997 and 2003. Deep-Sea Res. 57 (5), 639–652. https://doi.org/10.1016/j.dsr.2010.03.005.

Rivaro, P., Ianni, C., Magi, E., Massolo, S., Budillon, G., Smethie Jr., W.M., 2015. Distribution and ventilation of water masses in the western Ross Sea inferred from CFC measurements. Deep-Sea Res. I 97, 19–28. https://doi.org/10.1016/j.dsr.2014.11.009.

Rivaro, P., Ardini, F., Vivado, D., Cabella, R., Castagno, P., Mangoni, O., Falco, P., 2020. Potential sources of particulate iron in surface and deep waters of the Terra Nova Bay (Ross Sea, Antarctica). Water 12 (12), 3517.

Robertson, R., 2005. Baroclinic and barotropic tides in the Ross Sea. Antarct. Sci. 17, 107–120. https://doi.org/10.1017/S0954102005002890.

Rubino, A., Budillon, G., Pierini, S., Spezie, G., 2003. A. Model for the spreading and sinking of the deep ice shelf water in the Ross Sea. Antarct. Sci. 15, 25–30.

Rusciano, E., Budillon, G., Fusco, G., Spezie, G., 2013. Evidence of atmosphere–sea ice–ocean coupling in the Terra Nova Bay polynya (Ross Sea—Antarctica). Continent. Shelf Res. 61–62, 112–124. https://doi.org/10.1016/j.csr.2013.04.002.

Saji, N., Ambrizzi, T., Ferraz, S.E.T., 2005. Indian Ocean Dipole mode events and austral surface air temperature anomalies. Dynam. Atmos. Oceans 39, 87–101. https://doi.org/10.1016/j.dynatmoce.2004.10.015.

Sansiviero, M., Maqueda, M.M., Fusco, G., Aulicino, G., Flocco, D., Budillon, G., 2017. Modelling sea ice formation in the Terra Nova Bay polynya. J. Mar. Syst. 166, 4–25. https://doi.org/10.1016/j.jmarsys.2016.06.013.

Silvano, A., Foppert, A., Rintoul, S.R., Holland, P.R., Tamura, T., Kimura, N., Castagno, P., Falco, P., Budillon, G., Haumann, F.A., Garabato, A.N., Macdonald, A. M., 2020. Recent recovery of antarctic bottom water formation in the Ross Sea driven by climate anomalies. Nat. Geosci. 13 (12), 780–786. https://doi.org/10.1038/s41561-020-00655-3.

Simpkins, G.R., McGregor, S., Taschetto, A.S., Ciasto, L.M., England, M.H., 2014. Tropical connections to climatic change in the extratropical Southern Hemisphere: the role of Atlantic SST trends. J. Clim. 27, 4923–4936. https://doi.org/10.1175/JCLI-D-13-00615.1.

Sinclair, K.E., Bertler, N.A.N., Trompetter, W.J., 2010. Synoptic controls on precipitation pathways and snow delivery to high-accumulation ice core sites in the Ross Sea region, Antarctica. J. Geophys. Res. 115, D22112. https://doi.org/10.1029/2010JD014383.

Schmidtko, S., Stramma, L., Visbeck, M., 2017. Decline in global oceanic oxygen content during the past five decades. Nature 542, 335–33.

Smith, B., Fricker, H., Gardner, A., Medley, B., Nilsson, J., Paolo, F., 2020. Pervasive ice sheet mass loss reflects competing ocean and atmos- phere processes. Science 368 (6496), 1239–1242. https://doi.org/10.1126/science.aaz5845.

Smith, S.D., Muench, R.D., Pease, C.H., 1990. Polynyas and leads: an overview of physical processes and environment. J. Geophys. Res.: Oceans 95, 9461–9479.

Smith Jr., W.O., Sedwick, P.N., Arrigo, K.R., Ainley, D.G., Orsi, A.H., 2012. The Ross Sea in a sea of change. Oceanography 25, 90–103.

Smethie Jr., W.M., Jacobs, S.S., 2005. Circulation and melting under the Ross Ice Shelf: estimates from evolving CFC, salinity and temperature fields in the Ross Sea. Deep-Sea Res. I 52, 959–978.

Spezie, G., Manzella, G.M.R., 1998. The Oceanography of the Ross Sea (Antarctica). Spinger Verlag, p. 286, 88-470-0039-4.

Stammerjohn, S.E., Martinson, D.G., Smith, R.C., Yuan, X., Rind, D., 2008. Trends in Antarctic annual sea ice retreat and advance and their relation to El Niño-Southern Oscillation and Southern Annular Mode variability. J. Geophys. Res. 108, C03S90. https://doi.org/10.1029/2007JC004269.

Steig, E.J., Huybers, K., Singh, H.A., Steiger, N.J., Ding, Q., Frierson, D.M.W., Popp, T., White, J.W.C., 2015. Influence of West Antarctic ice sheet collapse on antarctic surface climate. Geophys. Res. Lett. 42, 4862–4868. https://doi.org/10.1002/2015GL063861.

Stevens, C., Hulbe, C., Brewer, M., Stewart, C., Robinson, N., Ohneiser, C., Jendersie, S., 2020. Ocean mixing and heat transport processes observed under the Ross Ice Shelf control its basal melting. Proc. Natl. Acad. Sci. USA 117 (29), 16799–16804.

Stewart, C.L., Christoffersen, P., Nicholls, K.W., Williams, M.J.M., Dowdeswell, J.A., 2019. Basal melting of Ross Ice Shelf from solar heat absorption in an ice-front polynya. Nat. Geosci. 12, 435–440.
Swadling, K.M., et al., 2023. Biological responses to change in Antarctic sea ice habitats. Front. Ecol. Evol. 10, 1073823. https://doi.org/10.3389/fevo.2022.1073823.
Swathi, M., Kumar, A., Mohan, R., 2023. Spatiotemporal evolution of sea ice and its teleconnections with large-scale climate indices over Antarctica. Mar. Pollut. Bull. 188, 114634. https://doi.org/10.1016/j.marpolbul.2023.114634.
Tamura, T., Ohshima, K.I., Nihashi, S., 2008. Mapping of sea ice production for Antarctic coastal polynyas. Geophys. Res. Lett. 35, L07606. https://doi.org/10.1029/2007GL032903.
Tamura, T., Ohshima, K.I., Fraser, A.D., Williams, G.D., 2016. Sea ice production variability in Antarctic coastal polynyas. J. Geophys. Res.: Oceans 121, 2967–2979. https://doi.org/10.1002/2015JC011537.
Thomas, R., Bentley, C., 1978. A model for Holocene retreat of the West Antarctic ice sheet. Quat. Res. (Tokyo) 10 (2), 150–170. https://doi.org/10.1016/0033-5894(78)90098-4.
Thomas, R.H., MacAyeal, D.R., 1982. Derived characteristics of the Ross ice shelf, Antarctica. J. Glaciol. 28 (100), 397–412. https://doi.org/10.3189/S0022143000005025.
Thompson, A.F., Stewart, A.L., Spence, P., Heywood, K.J., 2018. The antarctic slope current in a changing climate. Rev. Geophys. 56, 741–770. https://doi.org/10.1029/2018RG000624.
Thompson, D.W.J., Wallace, J.M., 2000. Annular modes in the extratropical circulation. Part I: month-to-month variability. J. Clim. 13, 1000–1016. https://doi.org/10.1175/1520-0442(2000)013.
Thompson, D.W.J., Solomon, S., 2002. Interpretation of recent Southern Hemisphere climate change. Science 296, 895–899. https://doi.org/10.1126/science.1069270.
Thompson, L., Smith, M., Thomson, J., Stammerjohn, S., Ackley, S., Loose, B., 2020. Frazil ice growth and production during katabatic wind events in the Ross Sea, Antarctica. Cryosphere 14, 3329–3347. https://doi.org/10.5194/tc-14-3329-2020.
Tian, L., Xie, H., Ackley, S., Tang, J., Mestas-Nuñez, A., Wang, X., 2020. Sea-ice freeboard and thickness in the Ross Sea from airborne (IceBridge 2013) and satellite (ICESat 2003–2008) observations. Ann. Glaciol. 61 (82), 24–39. https://doi.org/10.1017/aog.2019.49.
Tinto, K.J., Padman, L., Siddoway, C.S., Springer, S.R., Fricker, H.A., Das, I., Caratori Tontini, F., Porter, D.F., Frearson, N.P., Howard, S.L., Siegfried, M.R., Mosbeux, C., Becker, M.K., Bertinato, C., Boghosian, A., Brady, N., Burton, B.L., Chu, W., Cordero, S.I., Dhakal, T., Dong, L., Gustafson, C.D., Keeshin, S., Locke, C., Lockett, A., O'Brien, G., Spergel, J.J., Starke, S.E., Tankersley, M., Wearing, M.G., Bell, R.E., 2019. Ross Ice Shelf response to climate driven by thetectonic imprint on seafloor bathymetry. Nat. Geosci. 12 (6), 441–449. https://doi.org/10.1038/s41561-019-0370-2.
Tournadre, J., Bouhier, N., Girard-Ardhuin, F., Remy, F., 2016. Antarctic icebergs distributions 1992–2014. J. Geophys. Res.: Oceans 121, 327–349. https://doi.org/10.1002/2015JC011178.
Trumbore, S.E., Jacobs, S.S., Smethie Jr., W.M., 1991. Chlorofluorocarbon evidence for rapid ventilation of the Ross Sea. Deep-Sea Res. I 38, 845–870.
Turner, J., Maksym, T., Phillips, T., Marshall, G.J., Meredith, M.P., 2013. Impact of changes in sea ice advance on the large winter warming on the western Antarctic Peninsula. Int. J. Climatol. 33, 852–861. https://doi.org/10.1002/joc.3474.
Vaňková, I., Nicholls, K.W., Corr, H.F.J., 2021. The nature of ice intermittently accreted at the base of Ronne Ice Shelf, Antarctica, assessed using phase-sensitive radar. J. Geophys. Res.: Oceans 126, e2021JC017290. https://doi.org/10.1029/2021JC017290.
van Wijk, E.M., Rintoul, S.R., 2014. Freshening drives contraction of antarctic bottom water in the Australian Antarctic Basin. Geophys. Res. Lett. 41, 1657–1664.
Van Woert, M.L., 1999. Wintertime dynamics of the terra nova bay polynya. J. Geophys. Res. 104 (C4), 7753–7769. https://doi.org/10.1029/1999JC900003.
Verdy, A., Mazloff, M.R., 2017. A data assimilating model for estimating Southern Ocean biogeochemistry. J. Geophys. Res.: Oceans 122, 6968–6988.
Vichi, M., 2022. An indicator of sea ice variability for the Antarctic marginal ice zone. Cryosphere 16, 4087–4106. https://doi.org/10.5194/tc-16-4087-2022.
Visbeck, M., Thurnherr, A.M., 2009. High-resolution velocity and hydrographic observations of the Drygalski Trough gravity plume. Deep-Sea Res. 56, 835–842. https://doi.org/10.1016/j.dsr2.2008.10.029.
Wadhams, P., Aulicino, G., Parmiggiani, F., Persson, P.O.G., Holt, B., 2018. Pancake ice thickness mapping in the Beaufort Sea from wave dispersion observed in SAR imagery. J. Geophys. Res. 123, 2213–2237. https://doi.org/10.1002/2017JC013003.
Wang, G., Hendon, H.H., Arblaster, J.M., Lim, E.-P., Abhik, S., van Rensch, P., 2019. Compounding tropical and stratospheric forcing of the record low Antarctic sea-ice in 2016. Nat. Commun. 10, 13. https://doi.org/10.1038/s41467-018-07689-7.
Wang, X., Zhang, Z., Dinniman, M.S., Uotila, P., Li, X., Zhou, M., 2023. The response of sea ice and high-salinity shelf water in the Ross Ice Shelf Polynya to cyclonic atmosphere circulations. Cryosphere 17 (3), 1107–1126. https://doi.org/10.5194/tc-17-1107-2023.
Whitworth, T., Orsi, A.H., 2006. Antarctic bottom water production and export by tides in the Ross Sea. Geophys. Res. Lett. 33, L12609. https://doi.org/10.1029/2006GL026357.
Williams, W.J., Carmack, E.C., Ingram, R.G., 2007. Physical oceanography of polynyas. In: Smith, W.O., Barber, D.G. (Eds.), Polynyas: Windows to the World. Elsevier, Amsterdam, pp. 55–85.
Womack, A., Alberello, A., de Vos, M., Toffoli, A., Verrinder, R., Vichi, M., 2024. A contrast in sea ice drift and deformation between winter and spring of 2019 in the Antarctic marginal ice zone. Cryosphere 18, 205–229. https://doi.org/10.5194/tc-18-205-2024.
Yiu, Y.Y.S., Maycock, A.C., 2019. On the seasonality of El niño southern oscillation teleconnection to the Amundsen Sea region. J. Clim. 32, 4829–4845. https://doi.org/10.1175/JCLI-D-18-0813.1.
Yokoyama, Y., Anderson, J.B., Yamane, M., Simkins, L.M., Miyairi, Y., Yamazaki, T., Koizumi, M., Suga, H., Kusahara, K., Prothro, L.O., Hasumi, H., Southon, J.R., Ohkouchi, N., 2016. Widespread collapse of the Ross ice shelf during the late holocene. Proc. Natl. Acad. Sci. USA 113, 2354–2359.
Yuan, N., Ding, M., Ludescher, J., Bunde, A., 2017. Increase of the antarctic Sea Ice extent is highly significant only in the Ross Sea. Sci. Rep. 7, 41096. https://doi.org/10.1038/srep41096.
Zahriban Hesari, M., Inserra, G., Aulicino, G., Migliaccio, M., 2023. A spatio-temporal variability assessment of the C33 iceberg using multi-polarisation C-band SAR satellite data. In: 2023 IEEE International Workshop on Metrology for the Sea; Learning to Measure Sea Health Parameters (MetroSea). La Valletta, Malta, pp. 395–399. https://doi.org/10.1109/MetroSea58055.2023.10317507.
Zhang, L., Delworth, T.L., Yang, X., Zeng, F., Lu, F., Morioka, Y., Bushuk, M., 2022. The relative role of the subsurface Southern Ocean in driving negative Antarctic Sea ice extent anomalies in 2016–2021. Commun. Earth Environ. 3, 302. https://doi.org/10.1038/s43247-022-00624-1.
Zhang, C., Li, S., 2023. Causes of the record-low antarctic sea-ice in austral summer 2022. Atmos. Oc. Sci. Lett. 100353. https://doi.org/10.1016/j.aosl.2023.100353.